RICE UNIVERSITY

Electric Field Quenching of Single-Walled Carbon Nanotube Photoluminescence

by

Anton Viatcheslavovich Naumov

A THESIS SUBMITTED
IN PARTIAL FULFILLMENT OF THE
REQUIREMENTS FOR THE DEGREE

Master of Science

APPROVED, THESIS COMMITTEE:

R. Bruce Weisman

R. Bruce Weisman, Professor,
Chemistry

Douglas Natelson, Professor,
Physics and Astronomy,
Electrical and Computer Engineering,
Fellow, Rice Quantum Institute

Boris I. Yakobson, Professor,
Mechanical Engineering and Materials
Science, Department of Chemistry

Bruce Johnson, Distinguished Faculty
Fellow; Exec. Director of Rice Quantum
Institute
Department of Chemistry

HOUSTON, TEXAS

JUNE 2007

Abstract

The effect of an electric field on the photoluminescence of single-walled carbon nanotubes was investigated. Individual SWNTs embedded in polymeric film were deposited on microscope slides with electrodes. The fluorescence intensity and spectra of single semiconducting SWNTs were acquired. When SWNTs in polymer were subjected to electric fields of up to 10^7 V/m, a drastic decrease in their fluorescence intensity was observed. The effect was reversible and reproducible. SWNT fluorescence intensity was well approximated by inverse hyperbolic cosine of the electric field, with a single quenching parameter k. It was shown that the effect was induced by the electric field parallel to SWNT axis while the perpendicular component did not produce detectable quenching. The quenching process was found to be enhanced for long nanotubes. Bulk sample fluorescence studies indicated that the electric field quenching also becomes stronger with the decrease in bandgap energy. Potential theoretical models will be discussed.

ACKNOWLEDGEMENTS

My appreciation and acknowledgements go to the following people, whose invaluable contributions and support have led to present work.

Dr. R. Bruce Weisman, for his supervision, interest, and help regarding many aspects of my professional development, and for serving as a member of my thesis committee.

Members of the committee, Dr. Douglas Natelson and Dr. Boris I. Yakobson for their candid feedback, for their time and patience spent to read the thesis, and for serving as members of the thesis committee.

Dr. Sergei Bachilo, for his mentoring, insightful discussions, experimental assistance, support and friendship during years of my graduate education.

Dr. Dmitri Tsyboulski, for being a great colleague, mentor and friend, for offering many ideas, answering numerous questions and helping in many experiments.

And finally, former and current members of the R. B. Weisman group: John-David Rocha, John Casey, Tonya Leeuw, Paul Cherukuri and Saunab Ghosh for their help, criticism, and for being great colleagues to work with.

TABLE OF CONTENTS

LIST OF FIGURES

1. Introduction

1.1 General Introduction

Currently a significant part of leading scientific research is conducted in the areas of Bio- and Nanotechnology. A number of recent publications have depicted technological and scientific advances in these areas. It has been shown that single-electron transistors can serve as efficient biological sensors[1] determining the presence of many possible diseases at once, whereas ZnO nanowires and carbon nanotubes can be used as field emitters for new technology flat panel displays[2-4]. Also a significant number of publications concern the study of novel nanomaterials such as fullerenes[5], nanowires[6;7] nanorods, nanoshells, and carbon nanotubes.

1.2 Introduction into Carbon Nanotubes

Both fullerenes and carbon nanotubes can be considered as different conformations of carbon. Their unique properties are determined by their structure. A single carbon nanotube can be represented as a graphene sheet rolled up in a cylinder (Fig 1). Due to the fact that graphene sheet wrapping can happen along various directions there can be several resulting structures of single-walled carbon nanotubes. Each is defined by the coordinates of its chiral (wrapping) vector. These coordinates, represented by indices n and m, indicate how many lattice vectors a_1 and a_2 of the graphene lattice are needed to construct a particular chiral vector. For example, as seen from Fig 1.a, to construct the chiral vector of (9,4) carbon nanotube, one would need to add up nine a_1 and four a_2 vectors.

The nanotube's diameter is the length of chiral vector divided by π. The other structural parameter is the chiral angle, between the chiral vector and a basis vector a_1. It varies between 0 and 30 degrees. SWNTs with chiral angle of 0° are called zigzag structures whereas those with chiral angle of 30° are armchair structures.

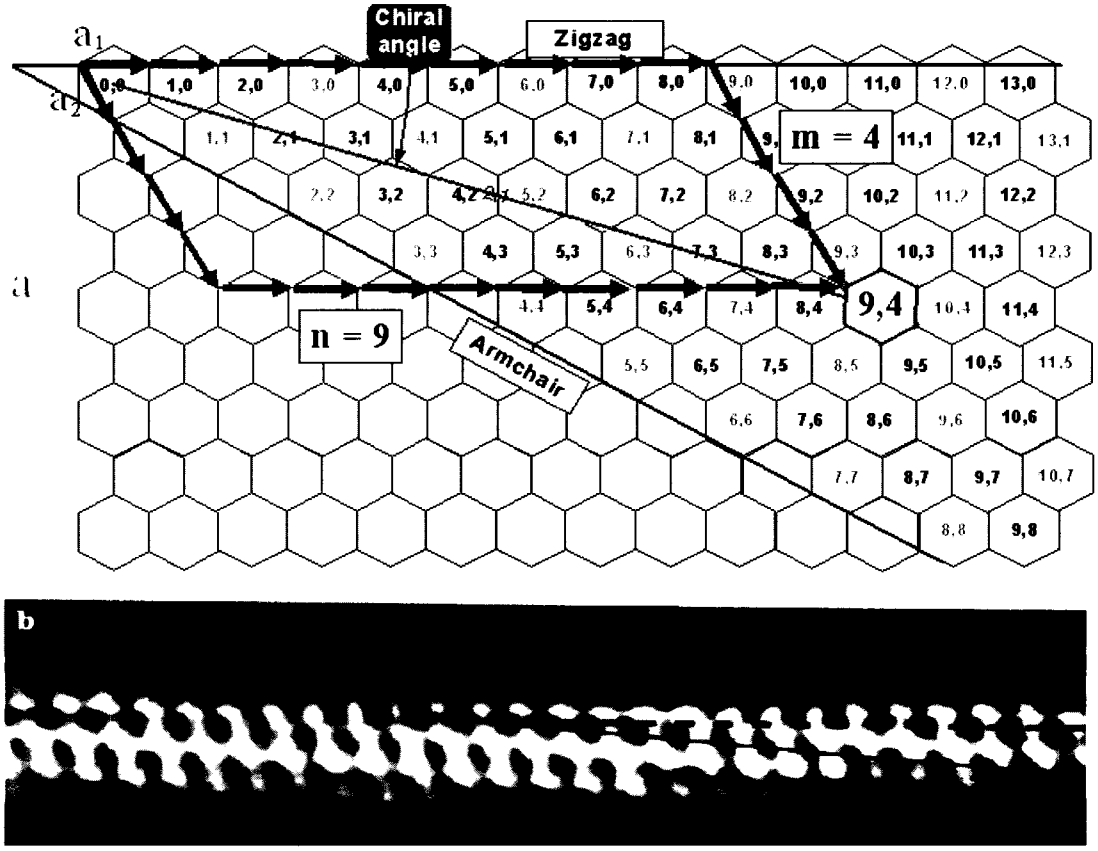

Figure 1. a – carbon nanotube roll up diagram; b – STM image of chiral SWNT[8].

1.3 Carbon Nanotube Band Structure

Depending on their structure, carbon nanotubes can be classified as metallic or semiconducting. Tight Binding calculations[9] show that the nanotubes for which n-m is divisible by 3 have no bandgap (their valence and conduction bands intersect at one

point), so they can be considered metallic. Other carbon nanotubes have a 1 – 2 eV gap between their valence and conduction bands and therefore are semiconducting (Fig. 2). It is predicted that 1/3 of the total number of carbon nanotubes are metallic[10]. For example, all armchair single-walled carbon nanotubes are metallic due to the fact that their n-m is equal to zero.

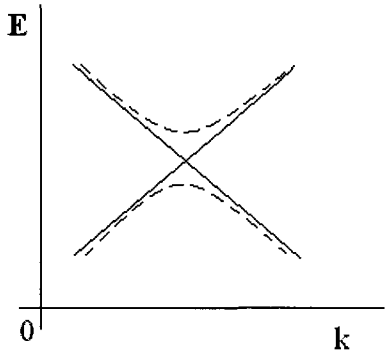

Figure 2. Band structure of semiconducting (dashed line) and metallic (solid line) carbon nanotubes.

Due to their 1-dimensional structure, both metallic and semiconducting carbon nanotubes exhibit sharp peaks in their density of states called van Hove singularities (Fig. 3). The density of states between c_1 and v_1 subbands for metallic carbon nanotubes is nonzero (Fig 3. a), therefore they have no band gap. As for semiconducting nanotubes, the band gap is represented by the separation between the first valence (v_1) and first conduction (c_1) subbands (Fig 3. b). Band gap energies E_{11} scale approximately inversely with carbon nanotube diameter.

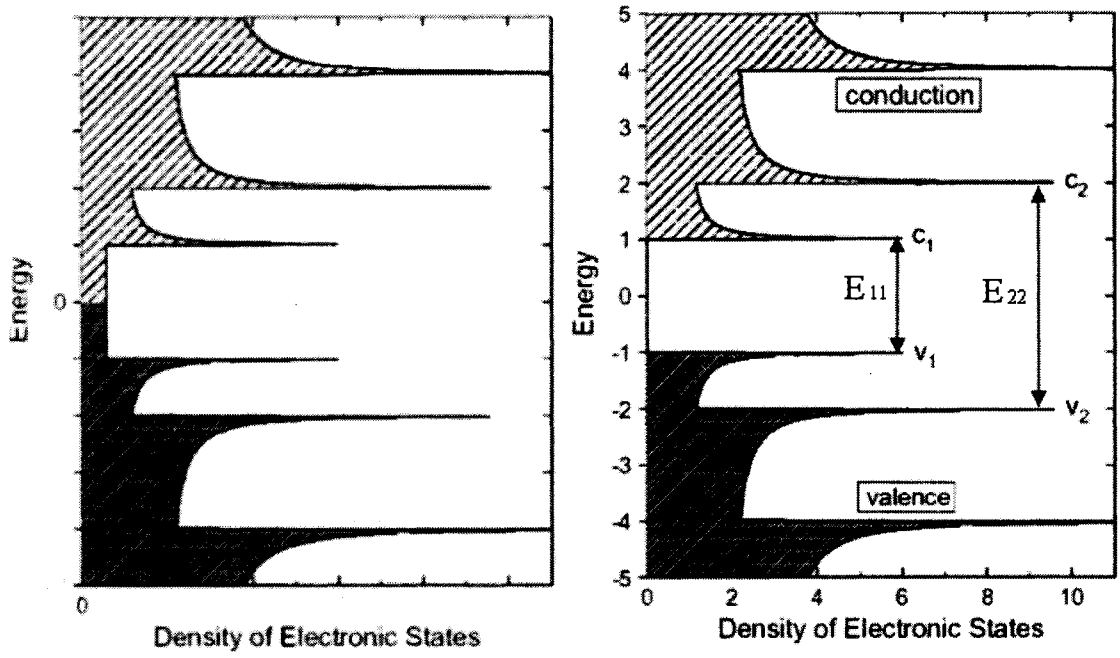

a. b.

Figure 3. a - density of states of metallic carbon nanotube; b - density of states of semiconducting carbon nanotube[11].

1.4 History and Development

Carbon nanotubes were discovered in 1991 in Japan[12]. At first, multi-walled nanotubes were found in arc discharges and later on in 1993 single-walled carbon nanotubes were discovered[13]. Several other current methods of carbon nanotube production include Chemical Vapor Deposition (CVD), where carbon-based gas is deposited in a form of nanotubes on catalytic substrate; Laser Ablation, which is based on laser induced evaporation of graphite at high temperatures; and a relatively new technique called HiPco. HiPco stands for High Pressure Carbon Monoxide (CO). In this technique carbon nanotubes are produced by catalytic deposition of carbon monoxide gas

at high temperatures and pressures. The disproportionation of carbon monoxide on metal nanoparticles supplies material for nanotube growth.

One of the most challenging issues is how to determine what kinds of nanotubes come out of the reactor. Some of the best methods of carbon nanotube characterization are STM, Raman spectroscopy and photoluminescence spectroscopy. STM provides a well-resolved image of carbon nanotubes from which their length, diameter and chirality can ideally be determined. That technique is mostly useful for observing features of individual nanotubes. Raman spectroscopy offers a different way of characterization: carbon nanotubes were found to have diameter-specific breathing vibration modes that are active and resonance enhanced in Raman[9;14]. Therefore knowing the frequencies of the breathing mode peaks in Raman spectrum, one can determine the diameters of carbon nanotubes that are present in the sample and have electronic resonances near the Raman laser wavelength. Finally, one of the latest and most powerful characterization techniques is semiconducting carbon nanotube photoluminescence.

1.5 Carbon Nanotube Photoluminescence

The actual effect of carbon nanotube photoluminescence was discovered in 2001 by Prof. Weisman's group at Rice University[15]. They have studied carbon nanotubes in aqueous solution coated with sodium dodecyl sulfate (SDS) surfactant (Fig 4) that made nanotubes water-soluble. Surfactant coating together with intense ultrasonication prevented carbon nanotubes from aggregating into bundles. A centrifugation process was used to reduce the amount of catalyst particles and nanotube bundles in solution.

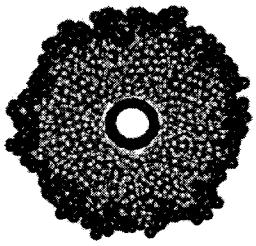

Figure 4. Model of a carbon nanotube suspended by SDS surfactant[15].

In their measurements of absorption and emission spectra of sonicated and centrifuged carbon nanotube solution, the authors found that emission spectral features corresponded directly to absorption features (Fig. 5). That showed that single-walled carbon nanotubes can exhibit so-called "bandgap photoluminescence"[15]. In that process optical excitation was followed by subsequent emission at E_{11}.

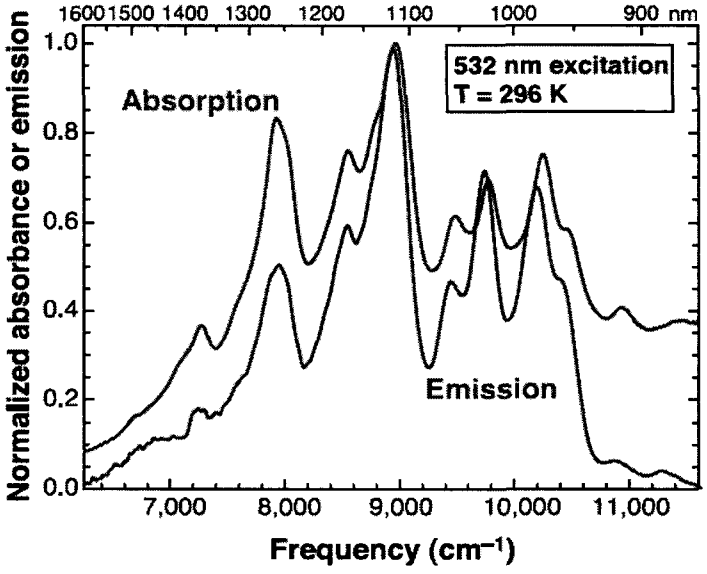

Figure 5. Absorption and emission spectra of carbon nanotubes in aqueous sodium dodecyl sulfate[15].

Different peaks in Fig. 5 were found to correspond to different structural types of carbon nanotubes. Therefore the main advantage of carbon nanotube photoluminescence is that it is highly structure-selective.

Following that work, Bachilo et al[11] have observed carbon nanotube photoluminescence for E_{22} excitation followed by E_{11} fluorescent emission (Fig. 6). In this process an electron from the second valence sub-band, v_2, gets excited to c_2 via the absorption of a photon. After that, the excited electron nonradiatively relaxes to c_1, losing its energy to vibrations. This is followed by its final radiative relaxation to v_1 with emission of a near infrared photon.

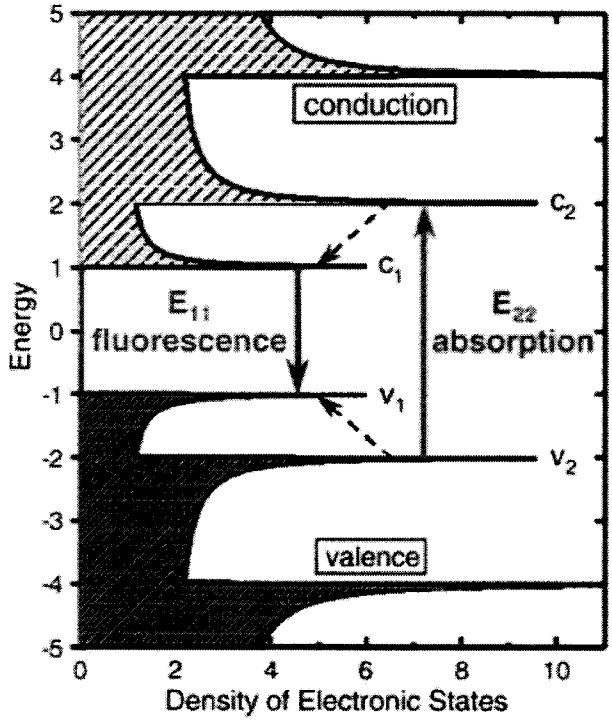

Figure 6. Carbon nanotube photoluminescence energy diagram[11].

The electron-hole pair that is formed in the excitation process can be considered as a separate entity, the exciton that is bound by Coulomb interaction. Due to quasi-one-

dimensional structure of carbon nanotubes, the binding energy of the exciton is relatively large[16]. That makes excitonic effects important in the optical transitions of carbon nanotubes[17] such as absorption[18] and photoluminescence.

In their paper, Bachilo et al have also shown that each type of single-walled carbon nanotube has a specific set of excitation and emission wavelengths. As seen from the figure 7, each bright spot on the excitation versus emission 2-D spectrum corresponds to a certain type of carbon nanotube with clearly defined n and m indices.

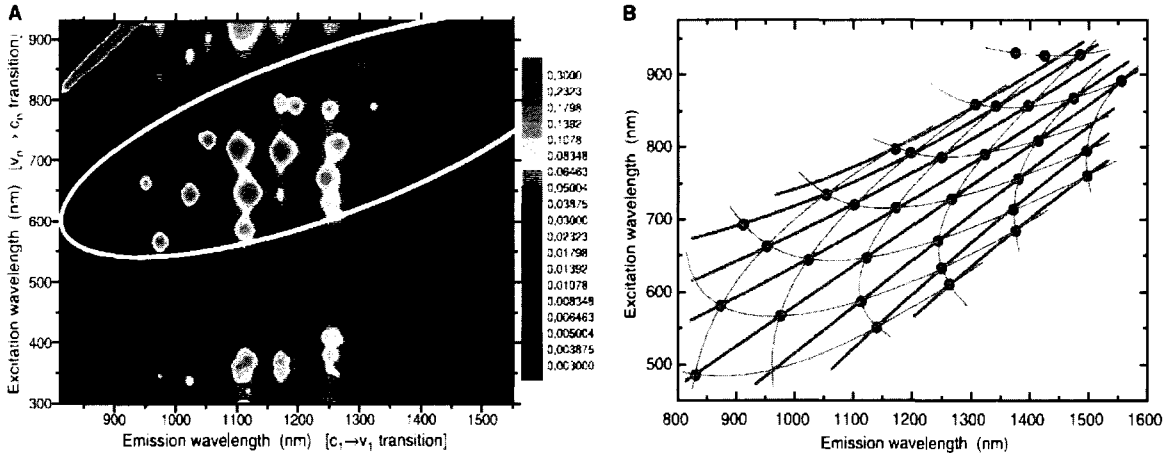

Figure 7. A – Photoluminescence intensity contour plot of excitation versus emission wavelength for carbon nanotubes[11]. B – Perceived structural patterns among the nanotubes in white oval on A.

That discovery was highly important, for it has shown that E_{11} and E_{22} energies were structure dependant, linking physical and electronic structures of single-walled carbon nanotubes. It can be clearly seen from Fig. 7 that bright spots (excitation/emission peaks) can be arranged in a certain pattern. Bachilo et al have studied possible structural arrangements that lead to such distribution of peaks on excitation/emission spectrum, dividing carbon nanotubes into several families according to their values of n and m.

Figure 7. B shows perceived patterns in the position of carbon nanotube photoluminescence peaks.

Actual assignments of n and m values to specific peaks on excitation/emission spectrum (Fig. 7) were made with a help of resonant Raman spectroscopy. As described above, SWNT Raman breathing modes depend on diameters of carbon nanotubes in the sample[9]. Authors have used that to pick several possible n,m assignments and choose between them optimizing the obtained model. As a result, each observed fluorescent peak was tagged with specific n,m values (Fig 8).

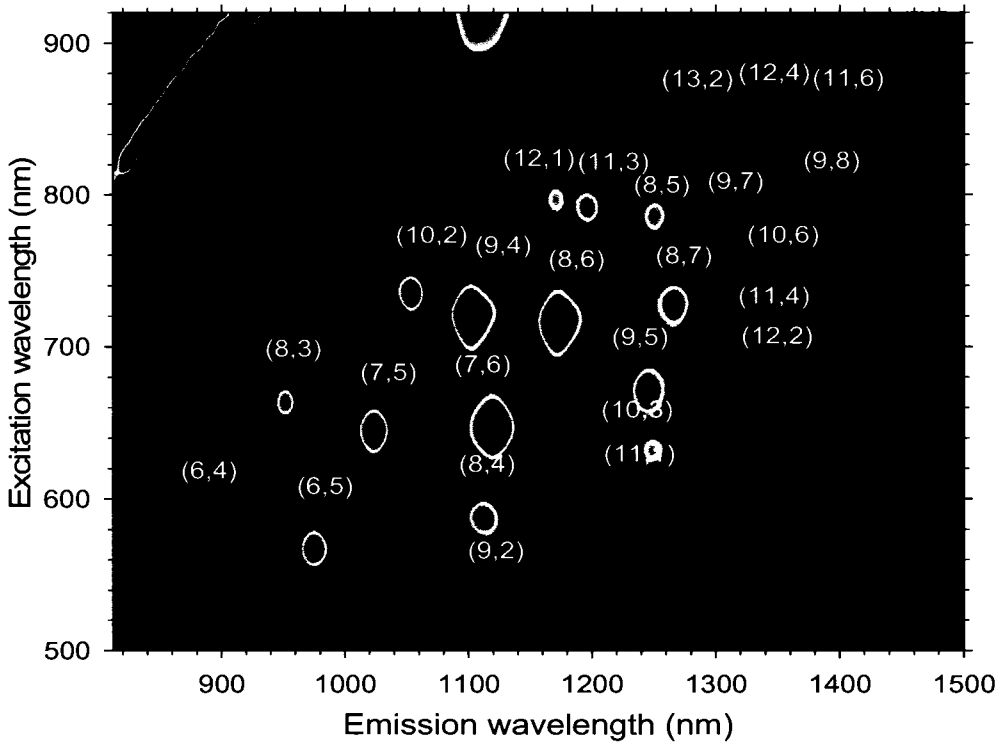

Figure 8. Structure–assigned SWNT fluorescence contour plot of excitation versus emission[11].

Such characterization opened the way to various revolutionary experiments that require the knowledge of the distribution of carbon nanotubes in the existing sample[19;20].

This method has found many applications since it is sufficiently reliable and easy to convey. For example, the dependence of carbon nanotube fluorescence on pH[21] or glucose concentration[22] can suggest a potential use of carbon nanotubes as biological sensors.

1.6 Overview

Due to their outstanding physical, electronic, and thermal[23] properties carbon nanotubes are currently a subject to intense research not only in the field of spectroscopy. Potentially, they can be used in different areas of science such as atomic force microscopy where carbon nanotubes are already being employed as AFM tips[24]. They are suitable for such applications due to their high Young's modulus on the order of one terapascal[25]. Carbon nanotubes can play an important role in future optics and electronics, serving as a basis for revolutionary nanoscale devices. Among such are ultrafast optical switches[26] and new generation field-effect transistors made from carbon nanotubes[27;28]. In these transistors carbon nanotubes serve as a semiconducting medium, a link between the source and a drain. Some of the devices have advanced to the point where the primary carriers in carbon nanotube could be selected by applying a bias of a certain sign[29]. Carbon nanotubes are also used as field emitters in electronic devices[3;4], where the applied field gradient detaches electrons off the end of a nanotube.

Currently there is a search for new applications related to interactions of electric fields with carbon nanotubes. Considering the importance of these effects, the properties of metallic and semiconducting carbon nanotubes in electric and magnetic fields have recently undergone theoretical investigation by a number of scientific groups[30-33]. It was

predicted [30;31;33] that applying a transverse electric field to semiconducting carbon nanotubes would cause a change in their bandgap, affecting the lifetime of the excited states and the probability of optical transitions. It was specifically pointed out that the applied electric field should shift the absorption peaks and increase their number by lowering degeneracy[34]. No experiments have been reported to test these theoretical predictions. We have therefore conducted an investigation of the effects of electric fields on SWNTs. Fluorescent spectroscopy of semiconducting carbon nanotubes[15] was used as a powerful tool for detecting fluorescence intensity variations or any significant shifts in nanotube energy level structure due to the applied electric field. This research was done via fluorescent imaging and nanotube emission spectroscopy.

Currently it is already possible to detect the fluorescence of individual SWNTs[35]. In such experiments near-infrared fluorescent microscopy is used to observe and characterize them by length, (n,m) identity, orientation in space, etc. Single-molecule spectroscopy opened a possibility for determining the electronic and optical properties of individual carbon nanotubes. Because of this advancement we have been able to study the behavior of individual carbon nanotubes in electric fields. Both longitudinal and transverse electric fields were used. Although no significant spectral shifts were found in the present work, dramatic decreases in fluorescence intensity of carbon nanotubes in electric field have been uncovered.

2. Experimental

2.1 Sample Preparation

Individual SWNTs spatially isolated in a poly(methyl methacrylate) (PMMA) matrix were obtained from the raw HiPco nanotube material. At first, HiPco carbon nanotubes were dispersed in water with addition of 1% Triton-X surfactant and bath sonicated for one hour in FS 145 Fischer Scientific bath sonicator. That suspension was then centrifuged at 12000g and the top decant was collected. That process helped to reduce the amount of nanotube bundles in solution: bath sonication broke large bundles and helped to mix carbon nanotubes with surfactant in water, whereas centrifugation precipitated heavy nanotube bundles that were later discarded. After that, a couple of drops of the suspension of nanotubes in aqueous Triton-X were added to ~5 % PMMA solution in o-xylene. The opaque product obtained after mixing water and xylene solutions was tip ultrasonicated using a Microson Ultrasonic Cell Disruptor at a power high enough to stimulate water evaporation. That was done with the purpose of randomly dispersing and incorporating SWNTs inside the PMMA matrix. Large ultrasonicator tips were used to deliver maximum power without damaging individual nanotubes. Due to the immiscibility of xylene and water and the fact that the boiling point of water (100°C) is lower then that of xylene (114°C), the water evaporated from the solution first. With no water present, the liquid became transparent. In addition to evaporating the water, tip ultrasonication facilitated dispersion of SWNTs in the PMMA solution and wrapping of SWNTs with PMMA molecules, which prevented SWNT aggregation as seen from SWNT fluorescence spectra. Two types of PMMA with molecular weights of 350,000

and 996,000 were used in experiments. The longer-chain polymer was considered more rigid and therefore more durable.

After such preparation several droplets of the low concentration SWNT suspension in PMMA/xylene were spin-coated onto a fused silica microscope slide with electrodes on it. During the process of spin-coating, the solvent quickly evaporated, leaving a clear PMMA film. These films which were several micrometers thick had individual SWNTs of submicron length embedded in them. The small thickness and high uniformity of the PMMA films was achieved by using relatively small concentrations of PMMA in o-xylene, giving a solution of a moderate viscosity that could spread uniformly over the slide with electrodes.

2.2 Electrodes

Two types of electrodes were employed in present experiments. First, we have used glass microscope slides coated with a thin highly transparent layer of ITO (Indium Tin Oxide). The films of PMMA with carbon nanotubes were deposited on the surfaces of two slides that afterwards were compressed together creating a parallel plate capacitor with a ~ 15μm PMMA-filled gap (Fig 9).

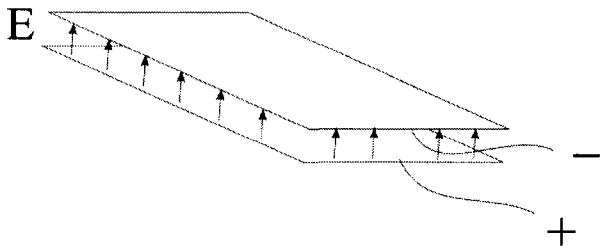

Figure 9. Parallel plate ITO electrodes.

In such a capacitor, carbon nanotubes in PMMA positioned between the plates were subject to electric fields of up to 20 V/μm. At higher voltages some film samples experienced breakdown. The main disadvantage of that configuration was that in the process of spincoating due to stretching of the film along the surface of a slide, most of the nanotubes in the film became oriented very similarly along the surface of the electrodes.

Several other configurations of electrodes were used. One of them consisted of a plastic film with an array of gold electrodes on it (Fig. 10).

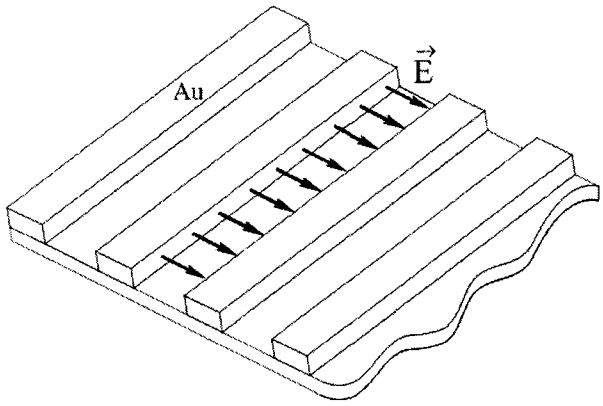

Figure 10. The array of gold electrodes on the plastic film substrate

The plastic substrate itself had a fluorescent emission in short-wavelength NIR, so a 1250 nm long-pass filter was used to block its fluorescence. The electrodes were represented by 50 μm wide gold stripes separated by 50 μm gaps and connected to two separate terminals. In such a configuration, voltages of up to 250 V were applied to electrodes creating fields on the order of several volts per micrometer between them. The piece of film with electrodes was attached to a microscope slide and spin-coated with nanotubes in PMMA.

Later on, a similar array of gold electrodes on a glass substrate was used. In these electrodes the gold stripes were 20 μm wide with 20 μm gaps between them. Since a glass substrate was used, the 1250 nm filter was no longer needed, so then one could observe the fluorescence of large diameter nanotubes farther in infrared.

Another configuration of electrodes was used to vary (rotate) the direction of the electric field for a certain nanotube situated between the electrodes. It consisted of four triangular electrodes with a gap of about 50x50 μm (Fig. 11). These electrodes were fabricated by depositing a nanometer layer of titanium and then a 15 nm layer of gold on the surface of the quartz slide. The triangular pattern of the electrodes was achieved by making two orthogonal scratches that removed the gold from the surface of the slide.

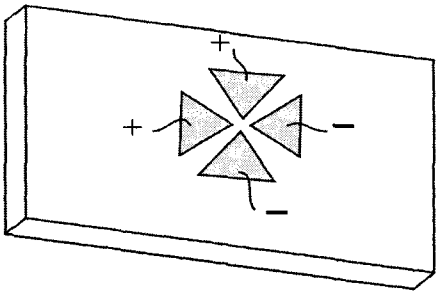

Figure 11. Triangular electrodes for variable field direction.

The nanotubes in the gap between the electrodes were subjected to electric fields at 0, 45 and 90 degrees. The direction of electric field was controlled by applying the voltage to certain electrodes or groups of electrodes. As a result, the electric field was rotated 360 degrees clockwise with angle increments of 45 degrees while carbon nanotube fluorescence was recorded.

2.3 Fluorescence Setup Apparatus

In the process of experiment the fluorescence of individual carbon nanotubes was constantly monitored to determine possible changes caused by the electric field. That was done using a standard fluorescence setup[35] (Fig. 12).

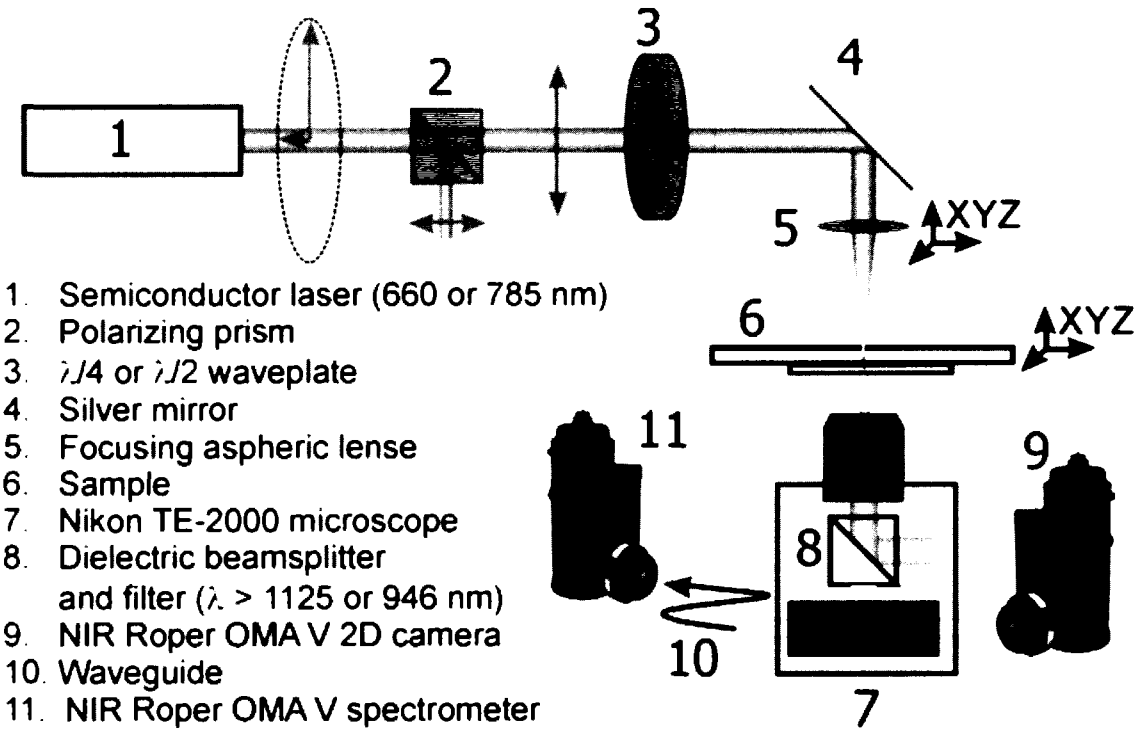

Figure 12. Fluorescence setup diagram[35]

In the setup, 785 nm or 660 nm semiconductor diode lasers were used as an excitation source. After a series of mirrors and a polarizer, laser light went through a half-wave retardation plate that rotated the polarization plane of oncoming light. This was done to determine the orientation of carbon nanotubes in PMMA with respect to the electrodes. It is known that carbon nanotubes exhibit the most efficient excitation when light is polarized along their axis. Therefore, the orientation of individual nanotubes in the plane of the film was determined by maximizing the fluorescent signal while rotating the excitation beam polarization with the half-wave retardation plate. After going through

the half-wave plate, the light was focused onto the sample by an aspheric lens. The lateral position of the focus could be adjusted manually. The sample itself was situated on a translation stage connected to a computer-controlled step motor.

The fluorescence from the sample of nanotubes in PMMA was collected by 60x water- or oil-immersion objectives on a Nikon TE-2000U inverted microscope and directed into one of five possible outputs. Two outputs were coupled respectively to an InGaAs NIR Roper OMA-V 2D camera and a NIR spectrograph equipped with an InGaAs Roper OMA-V array detector. The camera allowed us to observe the fluorescence of individual carbon nanotubes situated in between the electrodes, while the NIR spectrograph was used for recording the emission spectra of those nanotubes.

In that way, we were not only able to detect the fluorescence of individual carbon nanotubes (Fig 13) but also to determine their types through the spectra obtained[11;35]. The spectrum of a particular nanotube was recorded by moving it to a certain position on the screen (Fig 13) and accumulating the spectrum of that region (0.5x0.1 mm). The spectra were usually recorded as an average of 10 accumulations of 10 seconds each.

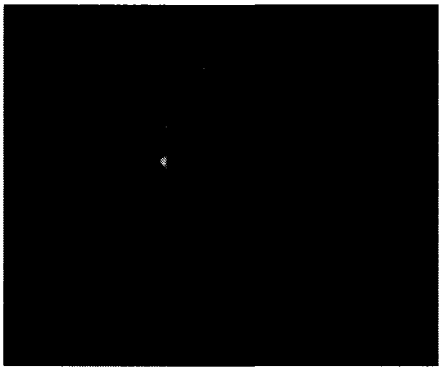

Figure 13. Image of carbon nanotubes in PMMA on NIR camera. Each bright spot represents an individual carbon nanotube or a small nanotube bundle.

The voltage was supplied to electrodes by a Tektronix AFG 2020 signal generator through a two-channel Trek 603 power amplifier with an output of up to 250 V. In experiments on carbon nanotube fluorescence quenching, DC voltage was used primarily.

2.4 Bulk Measurements

In addition to observing individual nanotubes we have also studied the bulk sample fluorescence of the films of carbon nanotubes in PMMA. These films were prepared as described above, only using highly concentrated PMMA in Xylene and nanotube solutions. Instead of spin-coating, polymer with large amount of carbon nanotubes imbedded in it was dried on a surface of a glass slide. As a result we obtained a rather thick ~0.5mm dark colored film of PMMA with carbon nanotubes embedded in it. Such film supplied enough signal for quantitative bulk sample fluorescence measurements. Later, the film was stacked between two ITO coated electrodes (Fig. 9) and subjected to electric fields of up to 2 V/μm.

The fluorescence of the film was recorded using a SPEX Fluorolog 3 spectrofluorometer with single-channel InGaAs detector (Fig. 14).

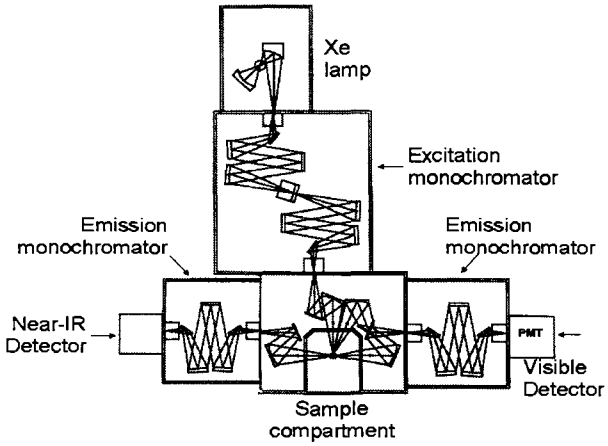

Figure 14. Diagram of SPEX Fluorolog 3 infrared spectrometer.

A Xe lamp served as an excitation source for most of the experiments. The light from the lamp went through a monochromator (Fig. 14) where a specific excitation wavelength was chosen to pass through the sample. Then spectrally selected luminescence from the sample was directed to a cooled InGaAs detector and presented in a form of fluorescence spectra containing peaks that represented multiple nanotube species present in the sample. Spectral changes under electric field were observed and analyzed. When a high fluorescence signal was necessary to obtain precise quantitative measurements, 980 or 655 nm diode lasers were used as excitation sources.

3. Results

3.1 SWNT Fluorescence Intensity Quenching in the Electric Field

The effects of the electric field on carbon nanotube photoluminescence were observed with a setup described above. First, the fluorescence of individual carbon nanotubes was studied using ITO-coated microscope slides as electrodes (Fig. 9). Further studies were conducted mostly with gold array electrodes for the reasons described below. In this series of experiments it was discovered that under electric fields of the order of several V/μm, the intensity of fluorescent emission of many carbon nanotubes drastically decreased (Fig. 15). Such fluorescence quenching was recorded at several values of the electric field. The effect was shown to be reproducible and highly reversible: when the voltage was turned off, the fluorescent intensity of carbon nanotubes restored almost to its initial value (Fig. 15).

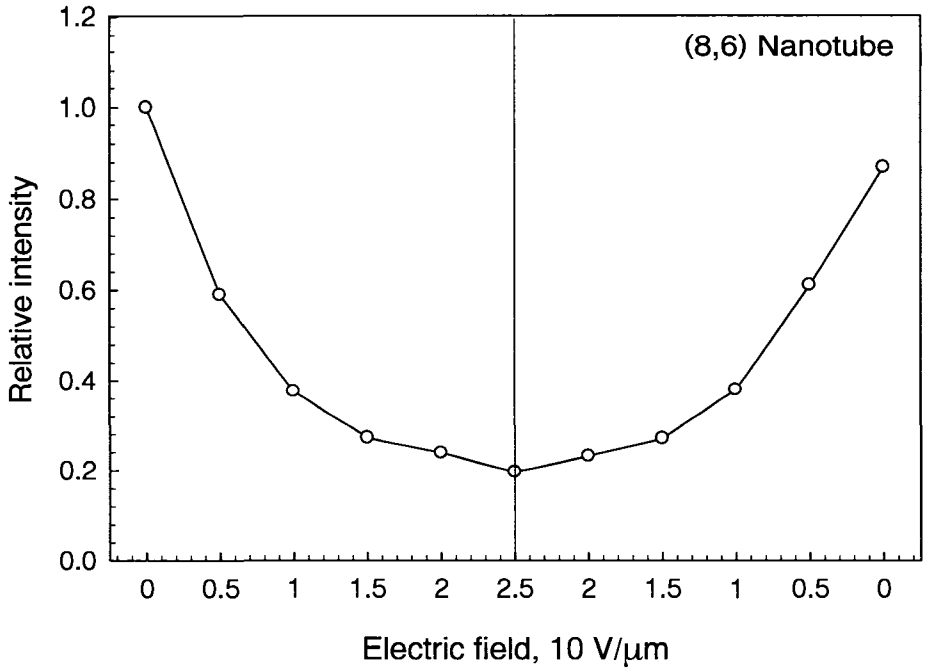

Figure 15. The quenching of the fluorescence intensity of one carbon nanotube as a function of applied field. Reversibility of the quenching is apparent.

Each fluorescence quenching curve was averaged over several runs and plotted versus increasing field (Fig. 16). Figure 16 represents the quenching curve of an (8,6) nanotube oriented at 50 degrees to the electric field. The nanotube type was determined from the spectrum. The inserts show 2-D fluorescent images of the nanotube at particular values of the electric field. One can infer from this graph that carbon nanotubes experience strong, nearly exponential fluorescence quenching at fields of ~ 1 V/μm. In fact, as seen from inserts, at higher fields it is hard to distinguish nanotube fluorescence from the background.

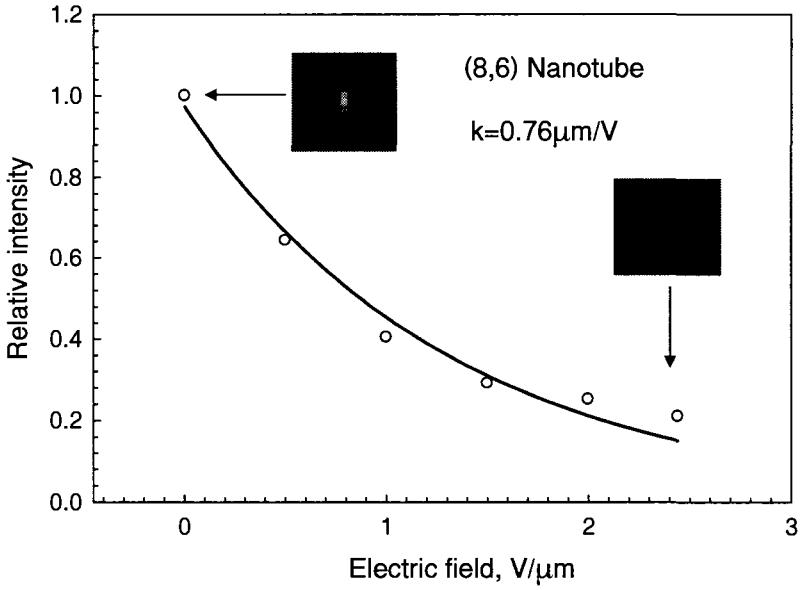

Figure 16. Carbon nanotube fluorescence quenching curve averaged over several runs and fitted with exponential function.

The quenching data on Fig. 16 were fit with a decaying exponential function (Eq. 1) with a parameter, k, that describes the steepness of the curve and therefore the sensitivity of carbon nanotube fluorescence intensity to applied electric field.

$$I = A \cdot \exp(-kE) \tag{1}$$

Several other fit functions were tried, including an inverse hyperbolic cosine (Eq. 2) that sometimes represented quenching curves better than simple Eq. 2. In Eq.2, k is again a quenching parameter that shows how much the fluorescence intensity decreases for a particular nanotube in electric field, E.

$$I = \frac{1}{A \cdot (\cosh(kE))} \tag{2}$$

As later studies have shown, out of several hundreds of SWNTs studied in this work the carbon nanotubes that experience weaker quenching at low fields exhibit behavior that resembles inverse hyperbolic cosine more than exponential (Fig .17).

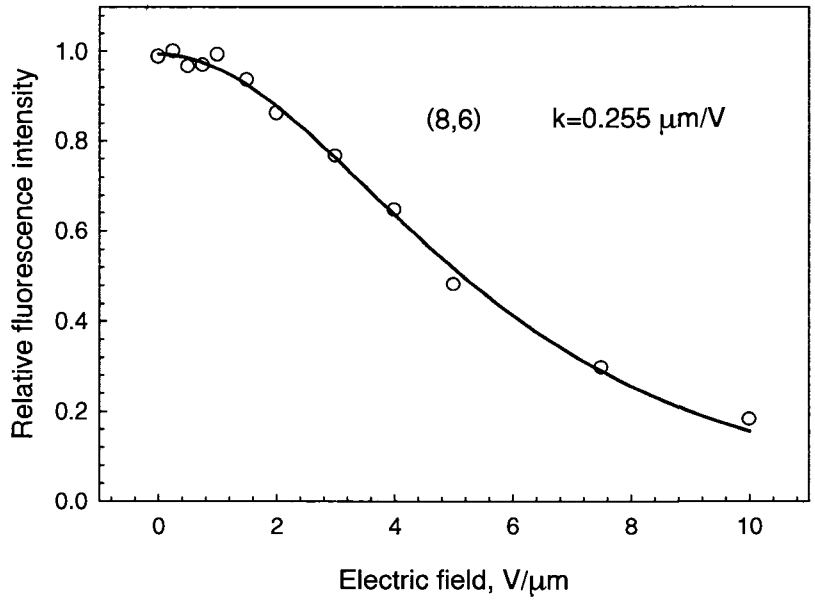

Figure 17. Inverse hyperbolic cosine fit of carbon nanotube fluorescence quenching curve.

As seen from Fig. 17, the first part of the curve could not be described by a simple exponential. Nevertheless, if one would apply higher electric fields at the beginning, or if the nanotube would be more sensitive to the electric field, then the flat part of the graph (Fig. 17) seen for fields of 0 to 1.5 V/μm would not show up, making the quenching curve appear reasonably exponential. That could explain why quenching curves for some nanotubes had profound exponential trends. For example, one can see that the carbon nanotube represented by Fig. 16 was very sensitive to the electric field: at small fields

around 1 V/μm the fluorescence was already quenched by 70%, which is reflected by the high quenching parameter k = 0.7631 μm/V. That implies that we have not observed a flat part of the quenching curve for that nanotube only because the quenching was already high at small fields, which made the curve look more like a decaying exponential. This example suggests that inverse hyperbolic cosine function may be used as a universal function to model carbon nanotube fluorescence quenching in electric fields.

3.2 Possible Theoretical Explanations.

There could be several theoretical explanations for the observed fluorescence quenching phenomenon. One possible model accounts for the direct effect of electric fields on excitons in carbon nanotubes. As presented before, the exciton could be considered as an electrostatically bound electron-hole pair with binding energies on the order of 400 meV[16]. When the electric field is applied, unless the nanotube is perpendicular to the field, the electron and the hole in the exciton are pulled toward opposite ends of the nanotube. Although fields of 1 V/μm are not enough to tear an exciton apart, they can increase the distance between the bound electron and hole. Statistically, the increased electron-hole separation would decrease the probability of radiative decay to give emission of an infrared photon. The separation of electron and hole in the exciton can also increase the probability of non-radiative decay of the exciton. Therefore the rate of fluorescent emission would go down and the fluorescence quantum yield would decrease.

Such a model can give a reasonable explanation for the shape of the quenching curve. We can assume that even without an applied electric field, each nanotube contains

a number of intrinsic quenchers that decrease the intensity of its fluorescent emission. Those could be charges trapped[36] at nanotube defects, creating high intrinsic fields or other sources of electric fields and temperature fluctuations that can affect a stability of an exciton. The destabilization of the exciton represented by Eq. 3 is created by pulling the electron away from the hole. We can write the simple model equation

$$\alpha = 2 \cdot b \cdot p \tag{3}$$

where α – exciton destabilization/separation rate,

b – attempt frequency. It represents the rate of attempts the electron tries to escape from the excitonic potential well. Due to high electron velocities the attempt factor is significantly large,

p – probability of electron motion in one direction. Since the electron motion is equally probable both ways along the nanotube, the factor of 2 is introduced.

When the electric field is applied (presumed along the nanotube axis), the probabilities of electron motion to the right and to the left would be different due to the force on the electron created by the field. This force would pull the electron more to one side than the other. Then equation 3 is modified into

$$\alpha = b \cdot p \cdot \gamma_1 + b \cdot p \cdot \gamma_2 \tag{4}$$

where γ_1 and γ_2 are the probability factors of electron motion to the right and to the left that increases the separation between the hole and the electron in the exciton.

Each probability was proposed to depend exponentially on the magnitude of the electric field, E, along the nanotube axis (Eq. 5) normalized by exciton binding energy E_b.

$$\gamma_1 = e^{(\varkappa\frac{E}{E_b})}, \qquad \gamma_2 = e^{(-\varkappa\frac{E}{E_b})} \tag{5}$$

Here $\varkappa$ represents the product of the charge of the electron and the separation of electron and hole in the exciton.

When we simplify the expression, the rate of exciton separation will be:

$$\alpha = b \cdot p \cdot (e^{(\varkappa\frac{E}{E_b})} + e^{(-\varkappa\frac{E}{E_b})}) = 2 \cdot b \cdot p \cdot \cosh(\frac{\varkappa E}{E_b}) \tag{6}$$

As mentioned above the increase in separation between electron and hole in electric field would most likely decrease the probability of exciton collapse and near-IR fluorescent emission. That would quench the intensity, I, of carbon nanotube photoluminescence. Therefore I should be inversely proportional to the rate of excitonic separation, α:

$$I \sim \frac{1}{b \cdot p \cdot (\cosh(\frac{\varkappa E}{E_b}))} \tag{7}$$

This resembles equation 2 for fluorescence quenching curve fits and thus shows the compatibility of the model described above with experimental results. According to this model quenching parameter k in Eq. 2 should be inversely proportional to the exciton binding energy E_b. Bulk spectral studies and theoretical calculations will be used to check this statement. Also, since in this mechanism only the projection of electric field along the nanotube axis pulls the exciton apart, k should depend also on the angle of the nanotube to the field. Experiments testing this point are described below.

Another possible contribution to carbon nanotube fluorescence quenching by electric fields could be quenching due to charge carriers. In the series of experiments it was shown that semiconducting carbon nanotubes acquire positive or negative charge

depending on the solvent they are suspended in. That was determined by placing carbon nanotubes in liquid solvents on the surface of gold array electrodes and observing them move to electrodes of only one particular sign when the electric field was applied.

Thus, if an exciton runs into a charge carrier, wether it is an electron or a hole, it can collapse and instead of emitting a photon give its energy to the carrier it ran into, promoting the carrier into a higher state in an Auger quenching process. That would decrease the intensity of the nanotube's fluorescent emission. Separation or dissociation of the excitons by the field, will contribute to this type of quenching since those processes create additional charge carriers.

When an electric field is applied, the charges that were previously trapped[16] in defects or weakly bound in other manners become mobile and drift towards the ends of the nanotube. Then, due to accumulation of charged carriers on the ends of carbon nanotube, they can induce greater fluorescence quenching at the ends, or particularly, at one end if as shown before there is an excess of a positive or a negative charge in the nanotube initially.

This predicted effect was observed experimentally in relatively long (3-4 μm) carbon nanotubes. That was possible because one could optically resolve the ends of those nanotubes and record the fluorescence intensity at each end as a function of the applied electric field. As a result of such measurements we have obtained a quenching curve for each end of a long (9,5) nanotube (Fig. 18) in the electric field. The direction of the electric field was varied by increasing voltage from -50 V to zero and then up to +50 V. Therefore, during that process the polarity of the electrodes was reversed.

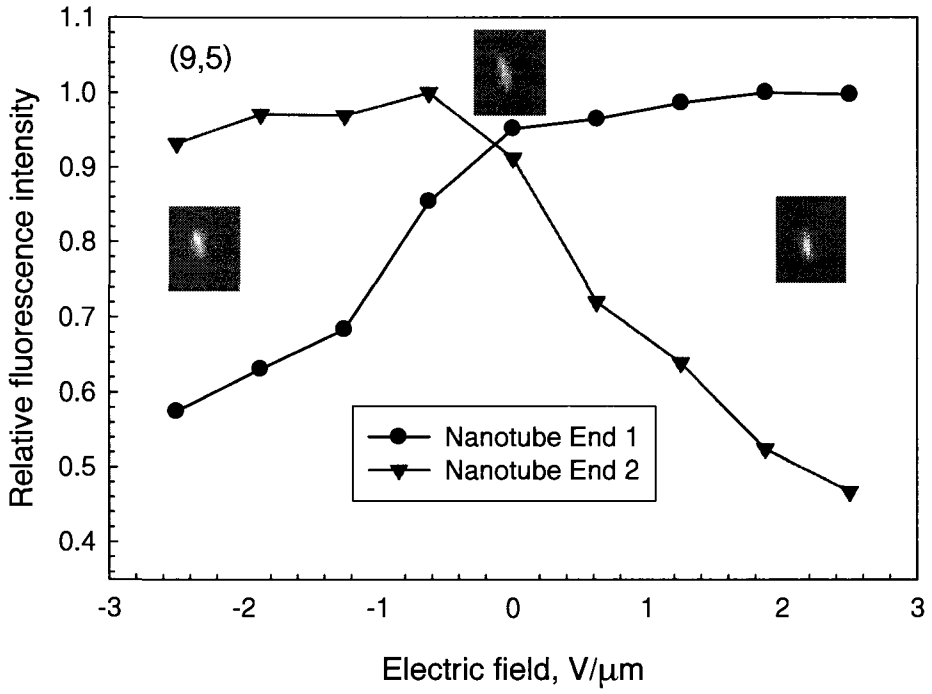

Figure 18. Fluorescence quenching for two ends of a long carbon nanotube. The inserts represent fluorescent image of a nanotube at particular values of electric field.

One can see from Fig. 18 that depending on the direction of the electric field different ends of carbon nanotube experienced a decrease in fluorescent emission intensity: end 2 quenched at positive voltages where as end 1 was quenched only when negative voltage was applied. In addition to that, end 1 experienced practically no quenching at positive voltages and end 2 experienced almost no quenching at negative ones. That could be explained according to the mechanism of charge carrier quenching as was mentioned above. It has been determined that carbon nanotubes possess some excess charge of a certain sign. Therefore in the presence of an electric field that positive or negative charge would gradually move towards one end of the nanotube and stay there, quenching carbon nanotube photoluminescence in that particular area. Therefore, when

the field is applied, one end of the nanotube would quench rapidly due to accumulation of charge carriers and the other end where charge carriers were mostly depleted would not quench at all. That explains what happened with the carbon nanotube in Fig. 18. When the direction of the field was reversed, the other end of the nanotube experienced severe fluorescence quenching as the carriers moved to the other end. That again is reflected in Fig. 18: when the field polarity is reversed, the opposite end of the nanotube quenches and the one that was quenched before recovers its fluorescence intensity. But even for that end of the nanotube it is still generally possible to see some intensity decrease due to the applied electric field. This may be accounted for by the other electric field fluorescence quenching processes present at the same time. As a result the decrease of fluorescent intensity at the ends of carbon nanotube depicted on Fig. 18 shows that charge carrier fluorescence quenching could be an important component of electric field induced fluorescence quenching in carbon nanotubes.

3.3 Angle Dependence

In a series of experiments it was determined that carbon nanotube fluorescence quenching in the measurements with ITO electrodes was significantly smaller then the one observed with gold array electrodes (Fig. 10). In the experiments with ITO electrodes, the fluorescence intensity decrease was just noticeable at 3.125 V/μm and became significant at about 18-25 V/μm, whereas in the case of using gold array electrodes, the fluorescence intensity was already quenched significantly at 2 V/μm. A possible reason for that difference could be that, as mentioned before, during the process of spin-coating SWNTs were mostly spread on top of ITO electrodes in the plane parallel

to them. That way, most of SWNTs appeared to be nearly perpendicular to electric field lines. In the case of the gold array electrodes, where the electric field was parallel to the substrate, after spin-coating carbon nanotubes were oriented at various angles to the field. This suggests that fluorescence quenching effect varied with the angle of carbon nanotubes to the electric field, with smallest quenching observed when the electric field was perpendicular to the nanotube axis. It can be proposed then that only the component of electric field along the nanotube contributes to its fluorescence quenching. That idea is consistent with the exciton separation model described above: the exciton would be pulled apart only by the component of the field parallel to the nanotube axis.

To explore this point, the fluorescence of carbon nanotubes found at different angles to the field was studied. The experiments showed that with increasing angle between the nanotubes and the electric field lines, the rate of fluorescence quenching and, therefore, the quenching coefficient k, decreased. In a series of experiments, the quenching curves were recorded for several nanotubes at various angles to the field and their quenching coefficients were calculated using the inverse hyperbolic cosine approximation. The coefficients were then plotted versus the angle of carbon nanotubes to the electric field (Fig. 19).

Since carbon nanotube electric field fluorescence quenching is presumed to depend on the projection of electric filed along the nanotube axis, the expression for the quenching curve fit in Eq. 2 should be modified to:

$$I=\frac{1}{A\cdot(\cosh(-k_0\cdot\cos(\alpha)\cdot E))} \qquad \text{(Eq.8)}$$

where $\cos(\alpha)\cdot E$ is the projection of the electric field on the nanotube axis.

Thus, for any given E, quenching coefficient k would be represented as $k_0 \cdot \cos(\alpha)$ and therefore will depend on the cosine of the angle between the nanotube axis and the electric field. Such dependence was tested by fitting the data (k versus α) in Fig 19 with a cosine curve. The fit is very successful.

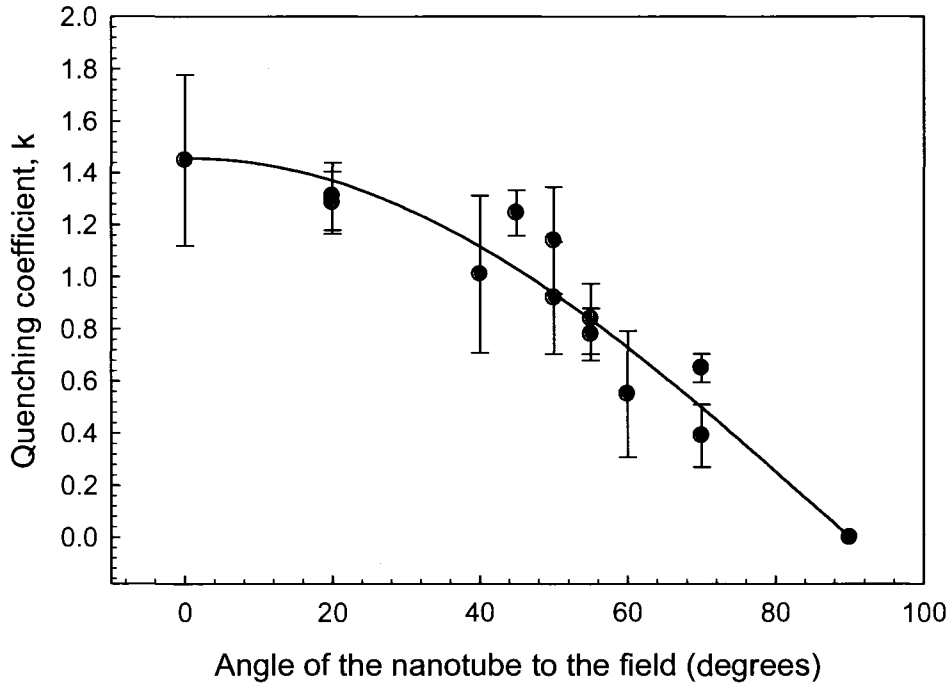

Figure 19. The cosine fit of the quenching coefficient dependence on the angle between carbon nanotube and the electric field.

Deviations from cosine behavior could be explained by the fact that quenching may also depend on some other parameters not controlled in that experiment. Among them are the presence of possible structural defects, carbon nanotube length and diameter that all vary from nanotube to nanotube. To eliminate those parameters in the measurements of the fluorescence quenching with respect to the angle of the nanotube to the field, we have conducted a series of experiments with electrodes fabricated

specifically for this purpose (Fig 11). These electrodes were used to rotate the electric field with respect to a stationary axis of one nanotube. The angle of the electric field was varied from 0 to 360 degrees in 45 degree increments. At each angle the fluorescence quenching at 50 V applied to electrodes was recorded. After the data were normalized and corrected for non-uniform distance from the nanotube to all four electrodes, they were fit to the absolute value of the cosine of the angle between the nanotube and the field (Fig. 20).

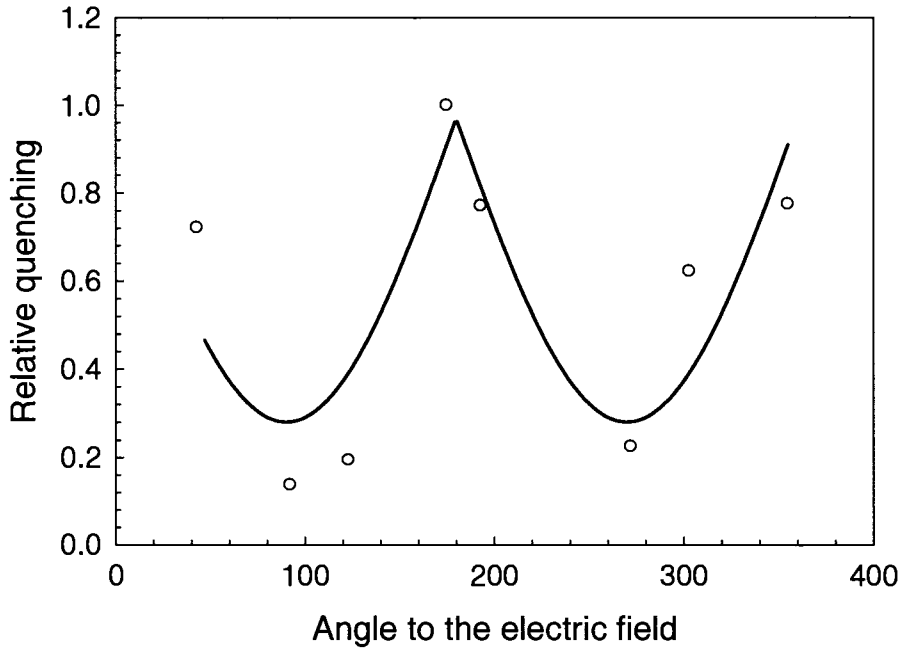

Figure 20. Single nanotube fluorescence quenching in the rotating electric field.

The data show an approximate $|\cos(\alpha)|$ pattern. The deviations from perfect cosine behavior could be caused by imperfections in the electrodes, fluctuations in the fluorescent intensity over time, possible defects and the presence of bundles, metallic nanotubes or particles around the nanotube.

Apart from uncontrolled parameters and imperfections in the data, figures 19 and 20 illustrate that carbon nanotube fluorescence quenching in the electric field is angle-dependent and that the quenching coefficient is proportional to the cosine of the angle between the nanotube and the electric field.

3.4 Length Dependence

Several experiments have been conducted with long carbon nanotubes incorporated in PMMA that were obtained from specific raw samples and subjected to very mild sonication to observe the dependence of the fluorescence quenching on the length of the nanotubes. Their quenching curves were compared (Fig. 21) to quenching of average-sized nanotubes of the same type and then analyzed.

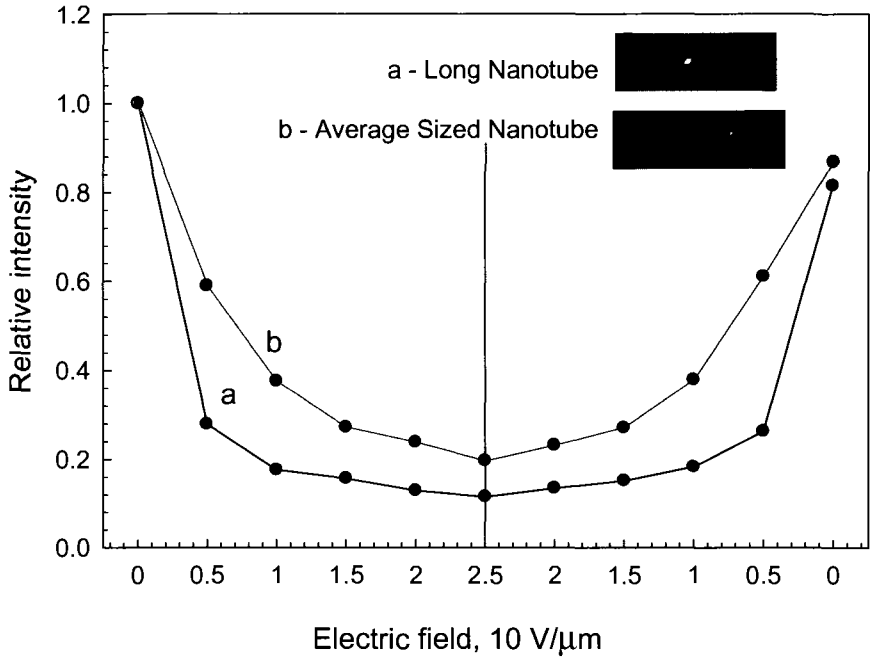

Figure 21. The electric field quenching of the fluorescence of long and average sized carbon nanotubes, both oriented at 50 degrees to the electric field. The inserts show fluorescence images of long and average carbon nanotubes between the electrodes.

It was possible to see from Fig. 21 that the longer nanotube experienced significant quenching at lower voltages until it reached some boundary where the quenching process slowed down, whereas the shorter one quenched more gradually. It seemed as if the longer nanotube was retaining some residual level of intensity, which was observed to be a common effect among long carbon nanotubes studied in our experiments.

The length dependence can be explained by the fact that longer nanotubes may have more quenchers such as charge carriers. The flat portion of the quenching curve can perhaps be accounted for by the fact that when the electric field is applied, the ends of the nanotube experience strong quenching as observed in the experiments (Fig. 18), whereas the middle retains a significant percent of the intensity. Then, at a certain voltage when the nanotube ends are quenched almost to zero and the fluorescence quenching happens only near the middle of the nanotube where charge carriers are sparse. Then the fluorescence quenching process slows down, resulting in a plateau on the quenching curve of the long nanotube (Fig. 21).

3.5 Diameter and Type Dependence

As for the dependence of fluorescence quenching on nanotube diameter, only several types of carbon nanotubes[37] could be observed using the 1250 nm filter with gold array electrodes on a plastic film. Therefore these studies were conducted with the bulk sample using ITO electrodes. The benefits of bulk fluorescence measurements were that both the angle and length dependences averaged out due to the large number of carbon nanotubes of various lengths and orientations in the sample. In addition to that, using

only one excitation wavelength one could see the spectrum containing several fluorescence peaks characteristic of different nanotube types. That way fluorescence quenching could be observed for several carbon nanotube species at once (Fig. 22).

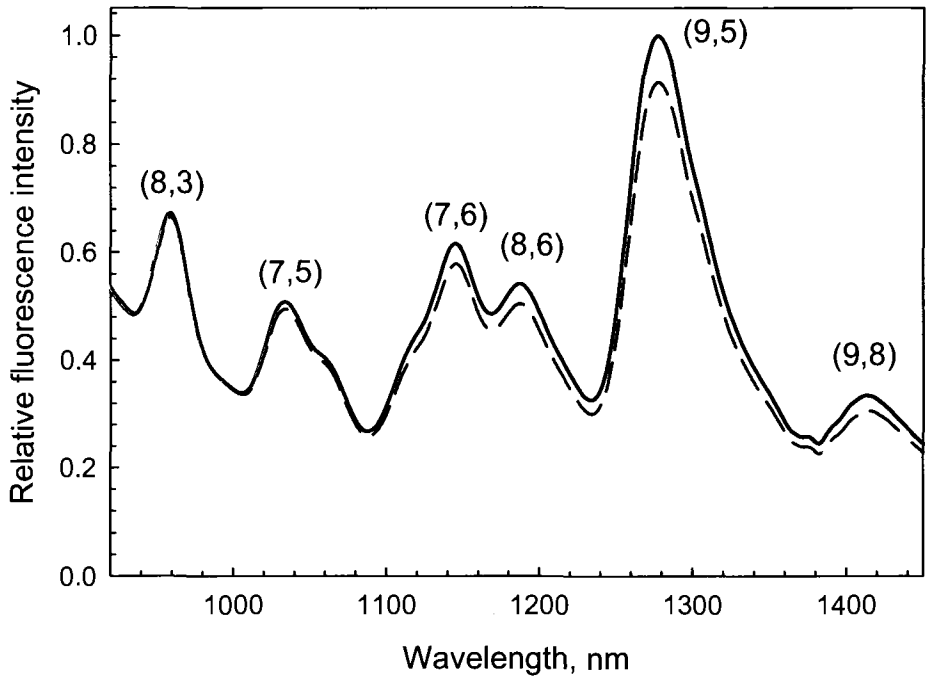

Figure 22. Bulk sample nanotube fluorescence spectra with 660 nm laser excitation. Solid curve – spectrum with no field applied. Dashed curve – spectrum of the carbon nanotube in an electric field of 2.273 V/μm.

As seen from Figure 22, carbon nanotube peaks experience different quenching at 2.3 V/μm. Two peaks on the left with lower emission wavelength experience almost no quenching at all, where as the ones to the right corresponding to emission from (7,6), (8,6) and (9,5) nanotubes are quenched significantly. Thus, Fig. 22 implies that carbon nanotubes with higher emission wavelength and, therefore, with greater diameter[37] experience more quenching in the electric field. This assumption was tested by measuring

fluorescence quenching for 12 carbon nanotube species at the field of 2.273 V/μm and plotting versus diameter of the nanotube (Fig. 23). Quenching measurements for each fluorescence peak corresponding to a particular nanotube type were made separately using appropriate excitation wavelengths.

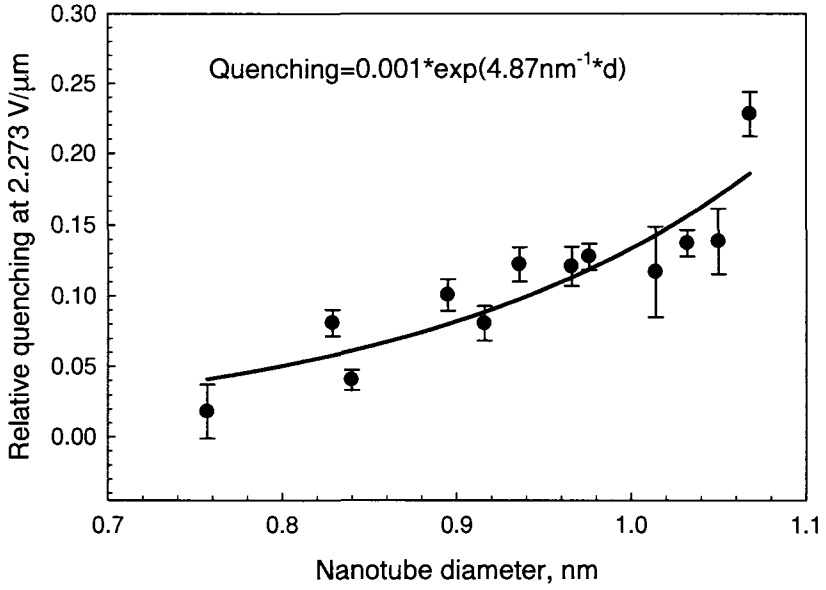

Figure 23. Carbon nanotube fluorescence quenching as a function of SWNT diameter.

One can see from Fig. 23 that the relative quenching of carbon nanotube fluorescence depends nearly exponentially on the diameter of the nanotube. Such a strong dependence indicates that SWNT diameter has a great influence on the fluorescence quenching process.

This matter was studied further to obtain the information about the nature of diameter dependence. First, the fluorescence intensity was recorded at several voltages for one particular spectral peak corresponding to emission from (9,5) nanotubes. The quenching curve was constructed (Fig. 24).

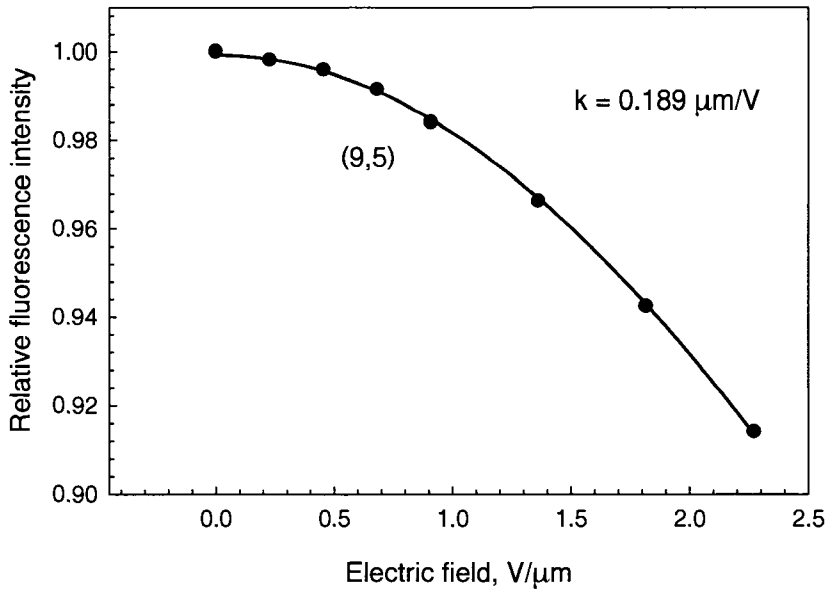

Figure 24. Fluorescence spectrum quenching of (9,5) nanotube .

The best fit for the curve on Fig. 24 appears to be a single parameter inverse hyperbolic cosine function with quenching parameter k = 0.1893 μm/V. This fit is similar to the one in (Fig. 17). The formula is the same and the only fact that makes these graphs look somewhat different is that in Fig. 17 a wider field range was used. If one would zoom in on the part of Fig. 17 that lies between 0 and 2.5 V/μm, it would look exactly like Fig. 24. Conversely if one would increase the voltage for nanotubes on Fig. 24, the quenching curve would most likely look like the one on Fig 17. That resemblance together with the simplicity of the fit involved showed that inverse hyperbolic cosine provides a successful model of carbon nanotube fluorescence quenching both for the bulk sample and for individual nanotubes. In addition to that, the presence of these inverse hyperbolic cosine trends in quenching curves is consistent with the exciton destabilization/separation model above.

Later on, quenching curves were measured for several types of nanotubes (Fig. 25) using selective excitation wavelengths and a lamp as an excitation source. Five nanotube fluorescence peaks were sampled.

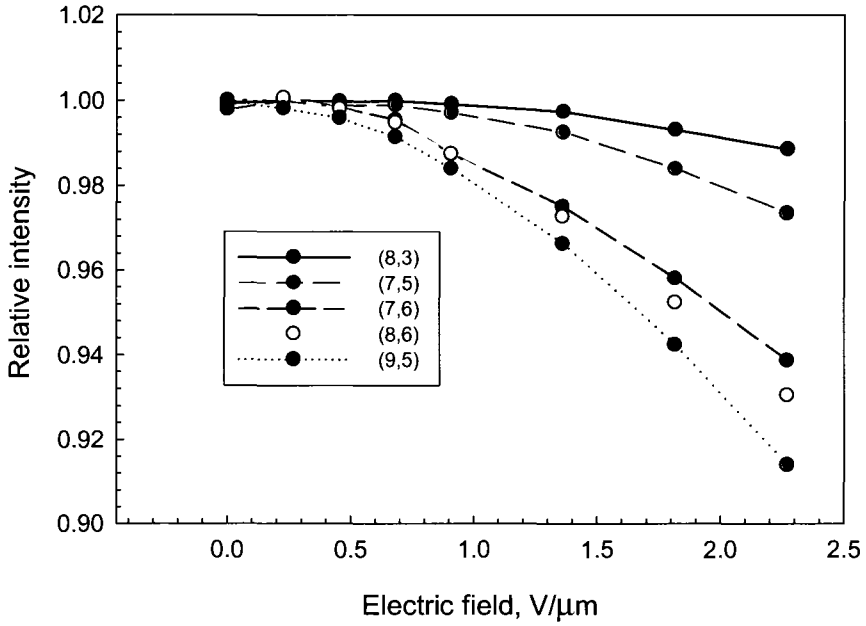

Figure 25. Quenching curves for five different types of nanotubes, lamp excitation. For these curves error bars are usually smaller then the point size.

Fig. 25 shows again that the strongest quenching, reflected by the steepness of the quenching curves, was observed for larger diameter (9,5) and (8,6) nanotubes. These curves were also fit with inverse hyperbolic cosine and the quenching coefficient for each of them was recorded. As a result, quenching coefficients for several types of nanotubes were plotted versus diameters of those nanotube species (Fig. 26). This analysis is more exact then the one represented in (Fig. 23) due to the fact that in this case we found fluorescence quenching at several values of the electric field instead of recording a relative quenching at just one point (2.273 V/μm).

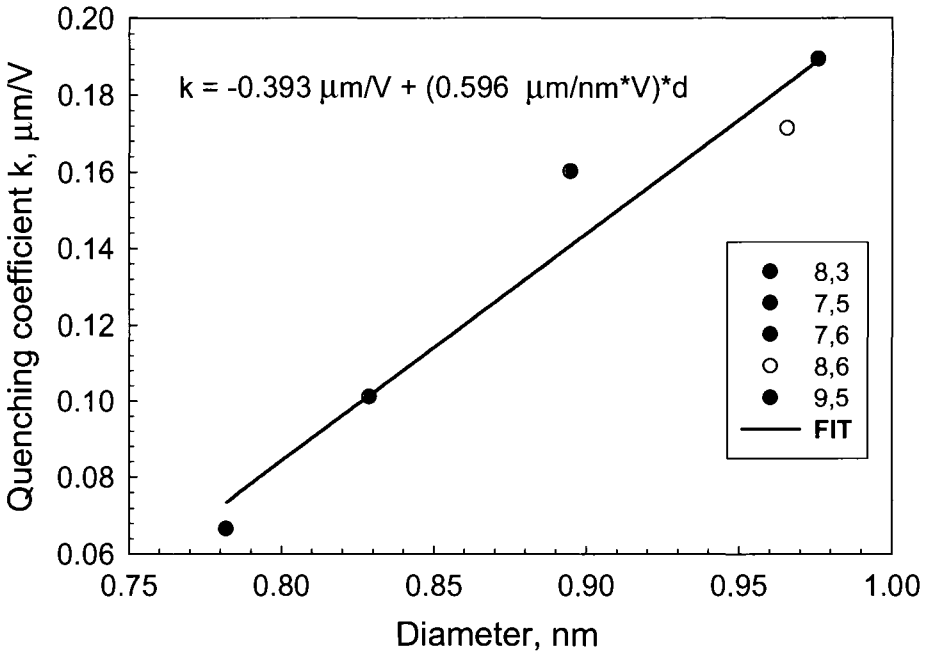

Figure 26. The dependence of the quenching coefficient on the diameter of the nanotubes for five different nanotube species.

Fig. 26 shows that the fluorescence quenching process depends strongly on the diameter of the nanotubes. Since the diameter of carbon nanotubes is known to be roughly inversely proportional to their E_{11} transition energy[37], the dependence of carbon nanotube fluorescence quenching on the magnitude of E_{11} energy was investigated. Using table data from the literature [37], it was discovered that the quenching coefficient had a linear dependence on E_{11} band gap energy (Fig. 27). This graph ties the nature of the quenching process with electronic structure of carbon nanotubes.

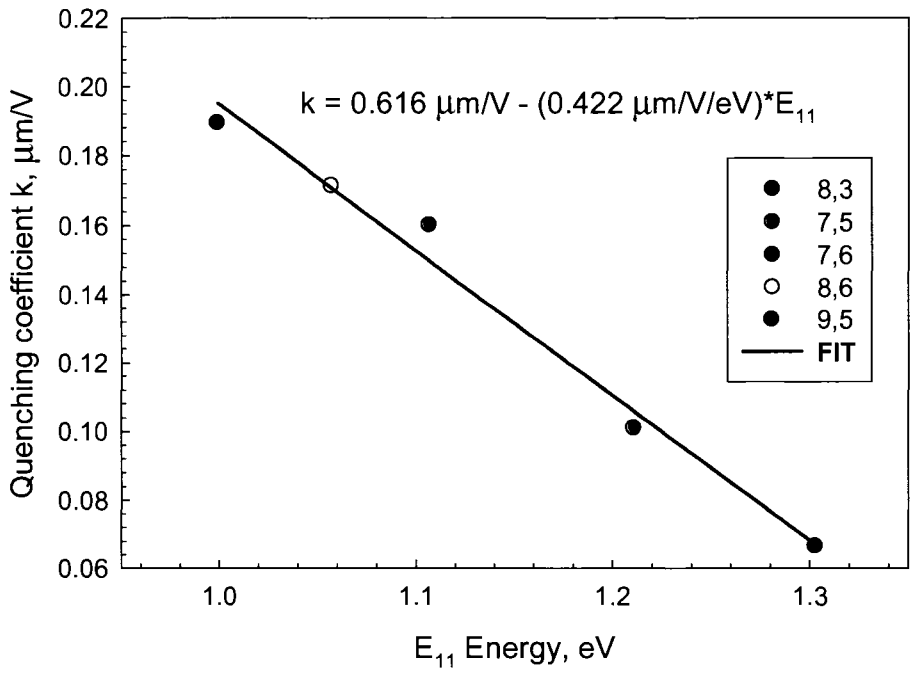

Figure 27. Dependence of carbon nanotube fluorescence quenching on E11 transition energy.

To understand the physical meaning of the observed effect in the framework of exciton destabilization/separation theory we have performed modeling of the exciton potential well in the presence of the electric field. Using a simple model that involves Coulomb interactions of an electron and hole on a cylindrical carbon nanotube of 1.1 nm diameter, the potential well of the exciton was calculated (Fig. 28). Dielectric screening and the effects of surrounding dielectric environment were taken into account by introducing an effective dielectric constant of 6 for carbon nanotubes.

The result appeared to be consistent with experimental results and calculations in ref. [16] where the binding energy of the exciton in a carbon nanotube was found to be 420 meV and electron-hole separation – on the order of 1.2 nm.

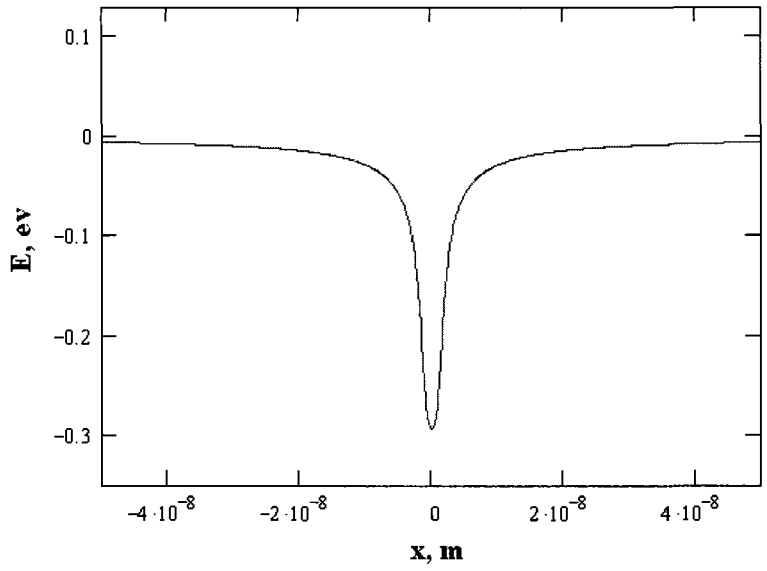

Figure 28. The potential well of an exciton with no electric field applied

As a next step in our calculations, when the electric field was applied it tilted the potential well (Fig. 29) making one of its walls somewhat thinner, and therefore, increasing of the probability of the separation/destabilization of the exciton.

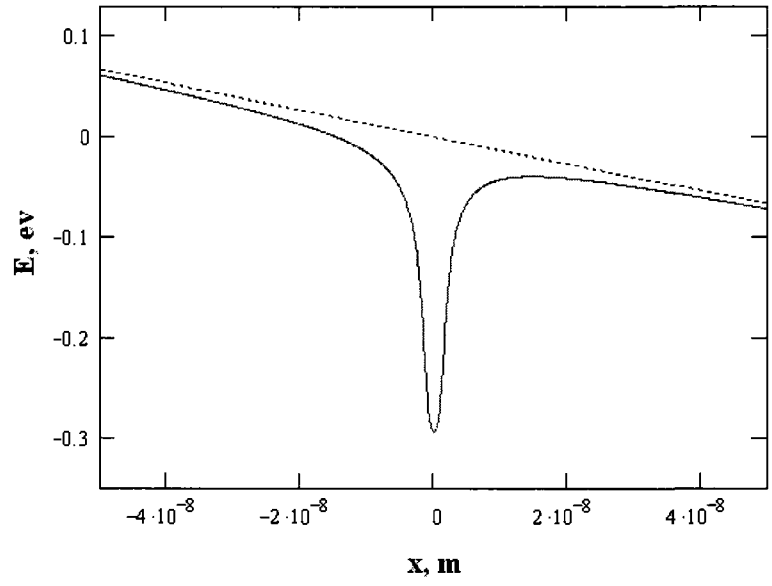

Figure 29. The potential well of an exciton with electric field of 4 V/μm applied.

As seen from Fig. 29, the barrier height is still substantial and the probability of total dissociation of the exciton through tunneling is low. That is why we focused on the potential separation of electron and hole under the electric field. However, if the dielectric constant of the nanotube is increased up to a value of 20, the potential well on Fig. 29 becomes shallower and the dissociation process becomes more probable.

In our model calculations, the binding energy of an exciton represented by the depth of the potential well appeared to depend on several factors. One of them was the diameter of the carbon nanotube, d. By calculating binding energies for several possible values of d, we have obtained a dependence of the exciton binding energy on the nanotube diameter (Fig. 30).

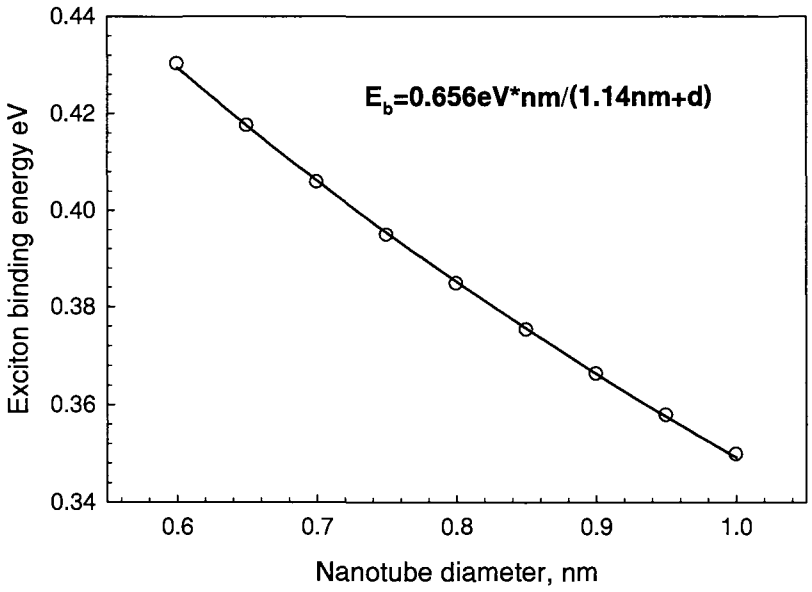

Figure 30. The dependence of calculated exciton binding energy on the diameter of the nanotube.

One can see that according to these calculations, binding energy of the exciton is inversely proportional to diameter of the nanotube, as it has also been also deduced in

more rigorous theoretical models[38;39]. That result is highly important, since electric field fluorescence quenching coefficients were experimentally found to be linearly proportional to the diameter of the nanotubes (Fig. 26). That suggests that the quenching coefficient will be inversely proportional to exciton binding energy. This finding supports the exciton destabilization/separation model, according to which the stronger the exciton is bound, the smaller would be the probability of pulling it apart. Therefore according to the model, the electric field fluorescence quenching and the quenching coefficient would be smaller for carbon nanotubes with strongly bound excitons. If the interpolation equations on both Fig. 30 and Fig. 28 are combined, the resulting equation (Eq. 9) would show the relation between quenching coefficient k and exciton binding energy.

$$E_b \approx \frac{0.3906 \frac{eV \cdot \mu m}{V}}{1.072 \frac{\mu m}{V} + k} \tag{9}$$

Using reasonable values of exciton binding energy in Eq. 9, one can obtain estimates of the quenching parameter, k, that are close to experimental values. This formula can be further improved by conducting series of quenching experiments complemented by more refined quantum mechanical modeling. It may then provide an important experimental route to exciton binding energies.

3.6 In-depth Study of the Carbon Nanotube Fluorescence Quenching Process and Electric Field Induced Spectral Shifts

Even though several possible quenching mechanisms were proposed above, it is still unclear wether the fluorescence quenching process happened while the excitonic electron was in c_1 or c_2 conduction sub-bands (Fig.6). To resolve this issue, a series of

experiments were conducted with bulk samples carbon nanotubes in PMMA. Two diode lasers with wavelengths of 660 and 980 nm were used to selectively excite (8,6) carbon nanotubes on E_{22} and E_{11} transitions respectively. It can be seen from (Fig. 6) that if E_{11} excitation is used the electron is promoted directly to c_1, where as in the case of E_{22} excitation it first enters the c_2 sub-band and then relaxes to c_1. Therefore, if the majority of the fluorescence quenching occurs in c_1, then the quenching curve obtained with E_{11} excitation would look just like the one for E_{22} excitation. On the other hand, if the quenching process mostly happened in the c_2 sub-band, the fluorescence quenching should be much less with E_{11} excitation than observed with E_{22} excitation. The analyses of carbon nanotube photoluminescence peaks recorded in the electric field using the Spex Fluorolog 3 instrument showed that quenching curves for E_{22} and E_{11} excitation exhibit similar behavior and their quenching coefficients are also close (Fig. 31). The 20% difference between k values suggests that a minor field induced quenching process may occur only for c_2 sub-band excitation. The major part of the fluorescence quenching, though, was carried out in c_1. That result was quite reasonable considering that the lifetime of electron in c_2 sub-band is low.

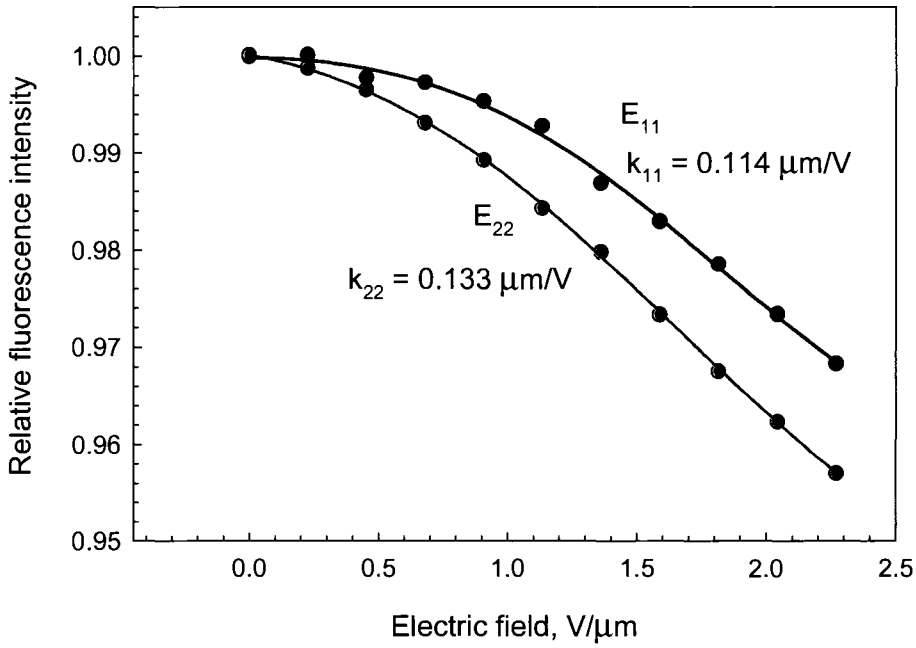

Figure 31. Quenching curves for E_{11} and E_{22} laser excitation of (8,6) nanotube.

One of the side goals of our experiments was to test prior predictions[30;31;33;34] that a transverse electric field would influence the electronic structure of a nanotube and therefore produce spectral shifts in carbon nanotube fluorescent emission. Such a possibility was considered and in single nanotube spectral measurements, red spectral shifts on the order of several nanometers were observed from time to time (Fig. 32). However, these shifts were not as large as predicted [30;31;33;34]. In addition, the observed effect was not common among all the nanotubes: some of nanotubes that were studied did not show any shifts at all; for some of them these shifts were not fully dependent on the electric field applied or even decreased at higher fields. So, at times the intensity of the peak decreased due to the fluorescence quenching effect, but its position as determined by peak fitting did not change (Fig. 33) or changed randomly.

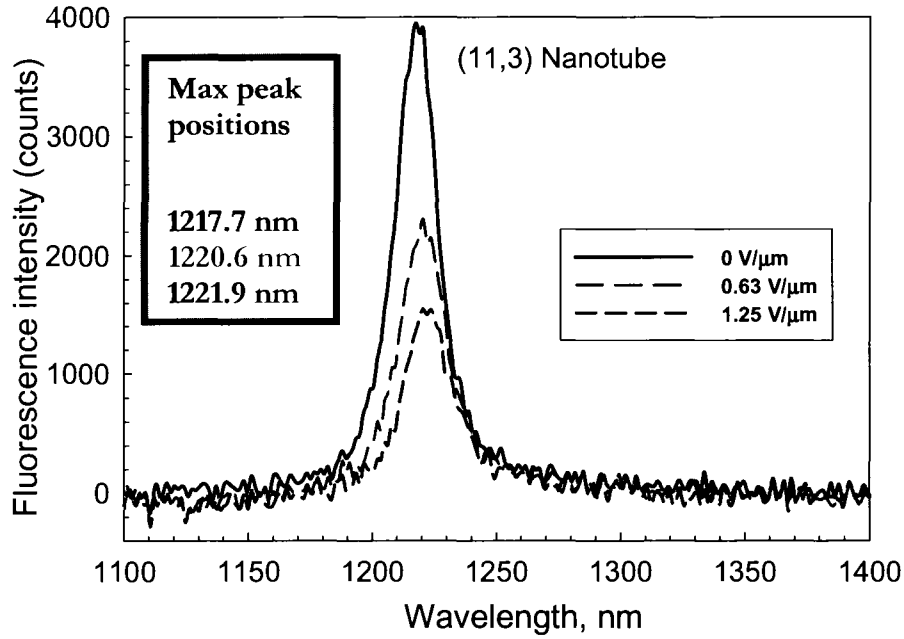

Figure 32. Fluorescence spectra of an individual nanotube in the electric field.

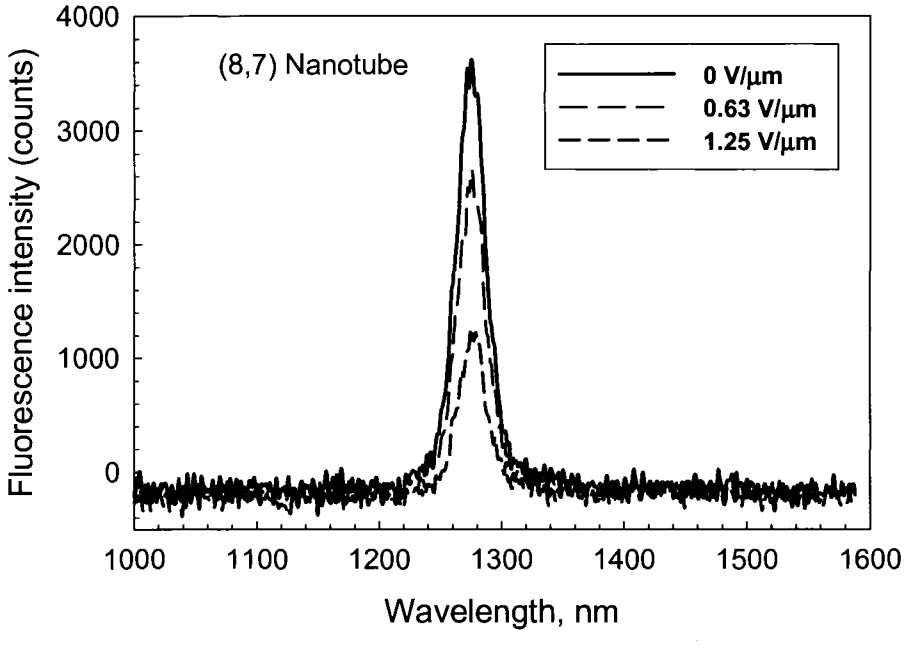

Figure 33. Fluorescence spectra of an individual nanotube in the electric field - no shift observed.

Such irregular behavior could be explained by the fact that the fields considered in the predictions[30;31;33;34] were substantially greater then the ones used here. Thus, it is possible that in our experiments due to low electric field strength the effect was small compared to experimental uncertainties. At much higher fields, it might be possible to observe more prominent spectral shifts that depend strongly on the electric field applied. That, together with specifics of temperature induced spectral shifts[40], can be a subject for further investigation.

4. Summary, Future Research and Possible Applications

In a series of experiments designed to detect possible variations in the electronic structure of carbon nanotubes is induced by electric fields, carbon nanotube fluorescence quenching was observed. The effect is clear and reproducible. At first, fluorescence intensity of carbon nanotubes in polymer was noticed to decrease reversibly with the electric field. After thorough investigation, carbon nanotube fluorescence quenching was found to follow an inverse hyperbolic cosine pattern characterized by a quenching parameter that reflected the steepness of the quenching curve.

It was experimentally determined that electric field fluorescence quenching observed in carbon nanotubes depends on the angle of the nanotube with electric field lines. Within experimental uncertainty, the quenching coefficient varied as a cosine of this angle for many individual nanotubes, as is consistent with our theoretical models of the fluorescence quenching effect.

Length of carbon nanotubes was also found to be an important factor influencing fluorescence quenching in the electric field. It was discovered that long carbon nanotubes experience strong quenching at low voltages and then reach a certain saturation level where the fluorescence intensity is nearly constant.

In addition to that, a strong dependence of carbon nanotube fluorescence quenching on the diameter of the nanotubes was detected. It was shown that SWNTs of larger diameters experienced more quenching than ones of smaller diameters and lower emission energy. Simple theoretical calculations were used to tie the observed effect with the concept of exciton binding energy and obtain a formula that can be used to deduce the binding energy of the exciton in carbon nanotubes from their fluorescence quenching and vice versa.

The effect of carbon nanotube fluorescence quenching in the electric field has several possible theoretical explanations. One of them is presented by the model based on the destabilization/separation of excitons in a longitudinal electric field. In that model partial separation of the exciton should decrease the fluorescence intensity of SWNT. That provides possible explanations of experimental findings concerning angle and diameter dependences of the quenching effect. Another potential mechanism is fluorescence quenching in the electric field caused by charge carriers inside the nanotube. The charge carrier quenching model provides an explanation of specific features of the quenching effect observed with long carbon nanotubes. It is also possible that the effect of carbon nanotube fluorescence quenching in the electric field is represented by a combination of several coexisting phenomena.

Further theoretical modeling based on quantum-mechanical calculations followed by possible absorption studies will be required to determine the actual nature of the observed effect. Among future research goals in this field are the investigation of influences of various environments with different temperatures and pH factors on electric field fluorescence quenching, the study of the nature of the phenomenon and the search for possible shifts in carbon nanotube fluorescence spectra caused by nanotube bandgap shrinkage at high electric fields[30;31;33;34]. Considering the temperature dependence of non-radiative decay processes, temperature related studies can show if the fluorescence quenching is partly triggered by an increase in non-radiative decay rate due to exciton separation in the electric field.

The effect of carbon nanotube fluorescence quenching can be applied in several areas of industry and science. It could be used in semiconductor electronics and in any device utilizing the concept of carbon nanotube fluorescence. For example, the dependence of SWNT fluorescence on applied electric field could be employed as a way to control the fluorescent emission of carbon nanotubes in nanoelectronic semiconductor photodevices. In addition, carbon nanotubes could be used as microscopic sensors of the electric field. The decrease in their fluorescence intensity can become an efficient way to obtain quantitative estimates of the electric field in a particular microscopic region.

Reference List

(1) Brousseau, L. C. *J.Am.Chem.Soc.* **2006**, *128*, 11346-11347.

(2) Lee, C. J.; Lee, T. J.; Lyu, S. C.; Zhang, Y.; Ruh, H.; Lee, H. J. *Appl.Phys.Lett.* **2002**, *81*, 3648-3650.

(3) Wang, Q. H.; Yan, M.; Chang, R. P. H. *Appl.Phys.Lett.* **2001**, *78*, 1294-1296.

(4) Lee, N. S.; Chung, D. S.; Han, I. T.; Kang, J. H.; Choi, Y. S.; Kim, H. Y.; Park, S. H.; Jin, Y. W.; Yi, W. K.; Yun, M. J.; Jung, J. E.; Lee, C. J.; You, J. H.; Jo, S. H.; Lee, C. G.; Kim, J. M. *Diamond and Related Materials* **2001**, *10*, 265-270.

(5) Kroto, H. W.; Heath, J. R.; O'Brien, S. C.; Curl, R. F.; Smalley, R. E. *Nature* **1985**, *318*, 162-3.

(6) Rao, C. N. R.; Deepak, F. L.; Gundiah, G.; Govindaraj, A. *Progress in Solid State Chemistry* **2003**, *31*, 5-147.

(7) Wu, Y.; Xiang, J.; Yang, C.; Lu, W.; Lieber, C. M. *Nature* **2004**, *430*, 61-65.

(8) Wildoer, J. W. G.; Venema, L. C.; Rinzler, A. G.; Smalley, R. E.; Dekker, C. *Nature* **1998**, *391*, 59-62.

(9) Saito, R.; Dresselhaus, G.; Dresselhaus, M. S. *Physical Properties of Carbon Nanotubes*; Imperial College Press: London, 1998.

(10) Saito, R.; Fujita, M.; Dresselhaus, G.; Dresselhaus, M. S. *Appl.Phys.Lett.* **1992**, *60*, 2204-2206.

(11) Bachilo, S. M.; Strano, M. S.; Kittrell, C.; Hauge, R. H.; Smalley, R. E.; Weisman, R. B. *Science* **2002**, *298*, 2361-2366.

(12) Iijima, S. *Nature* **1991**, *354*, 56-58.

(13) Iijima, S.; Ichihashi, T. *Nature* **1993**, *364*, 737.

(14) Dresselhaus, M. S.; Dresselhaus, G.; Jorio, A.; Souza Filho, A. G.; Saito, R. *Carbon* **2002**, *40*, 2043-2061.

(15) O'Connell, M.; Bachilo, S. M.; Huffman, C. B.; Moore, V.; Strano, M. S.; Haroz, E.; Rialon, K.; Boul, P. J.; Noon, W. H.; Kittrell, C.; Ma, J.; Hauge, R. H.; Weisman, R. B.; Smalley, R. E. *Science* **2002**, *297*, 593-596.

(16) Wang, F.; Dukovic, G.; Brus, L. E.; Heinz, T. F. *Science* **2005**, *5723*, 838-841.

(17) Ichida, M.; Mizuno, S.; Tani, K.; Saito, Y.; Nakamura, A. *J.Phys.Soc.Jpn.* **1999**, *68*, 3131-3133.

(18) Perebeinos, V.; Tersoff, J.; Avouris, P. *Phys.Rev.Lett.* **2005**, *94*.

(19) Bachilo, S. M.; Balzano, L.; Herrera, J. E.; Pompeo, F.; Resasco, D. E.; Weisman, R. B. *J.Am.Chem.Soc.* **2003**, *125*, 11186-11187.

(20) Lefebvre, J.; Fraser, J. M.; Homma, Y.; Finnie, P. *Appl.Phys.A* **2004**, *78*, 1107-1110.

(21) Strano, M. S.; Huffman, C. B.; Moore, V. C.; O'Connell, M. J.; Haroz, E. H.; Hubbard, J.; Miller, M.; Rialon, K.; Kittrell, C.; Ramesh, S.; Hauge, R. H.; Smalley, R. E. *J.Phys.Chem.B* **2003**, *107*, 6979-6985.

(22) Barone, P. W.; Baik, S.; Heller, D. A.; Strano, M. S. *Nature Mater.* **2005**, *4*, 86-92.

(23) Dresselhaus, M. S.; Dresselhaus, G.; Avouris, Ph. *Carbon Nanotubes: Synthesis, Structure, Properties, and Applications*; Springer-Verlag: New York, 2001.

(24) Hafner, J. H.; Cheung, C. L.; Oosterkamp, T. H.; Lieber, C. M. *J.Phys.Chem.B* **2001**, *105*, 743-746.

(25) Yakobson, B. I.; Campbell, M. P.; Brabec, C. J.; Bernholc, J. *Computational Materials Science* **1997**, *8*, 341-348.

(26) Chen, Y. C.; Raravikar, N. R.; Schadler, L. S.; Ajayan, P. M.; Zhao, Y. P.; Lu, T. M.; Wang, G. C.; Zhang, X. C. *Appl.Phys.Lett.* **2002**, *81*, 975-977.

(27) Martel, R.; Schmidt, T.; Shea, H. R.; Hertel, T.; Avouris, P. *Appl.Phys.Lett.* **1998**, *73*, 2447-2449.

(28) Tans, S. J.; Verschueren, A. R. M.; Dekker, C. *Nature* **1998**, *393*, 49-52.

(29) Chen, B. H.; Wei, J. H.; Lo, P. Y.; Wang, H. H.; Lai, M. J.; Tsai, M. J.; Chao, T. S.; Lin, H. C.; Huang, T. Y. *Sol.St.Elec.* **2004**, *50*, 1341-1348.

(30) O'Keeffe, J.; Wei, C. Y.; Cho, K. J. *Appl.Phys.Lett.* **2002**, *80*, 676-678.

(31) Pacheco, M.; Barticevic, Z.; Rocha, C. G.; Latge, A. *Journal of Physics-Condensed Matter* **2005**, *17*, 5839-5847.

(32) Rocha, C. G.; Pacheco, M.; Barticevic, Z.; Latge, A. *Brazilian Journal of Physics* **2004**, *34*, 644-646.

(33) Novikov, D. S.; Levitov, L. S. *Phys.Rev.Lett.* **2006**, *96*.

(34) Chen, R. B.; Lee, C. H.; Chang, C. P.; Lue, C. S.; Lin, M. F. *Physica E-Low-Dimensional Systems & Nanostructures* **2006**, *34*, 670-673.

(35) Tsyboulski, D. A.; Bachilo, S. M.; Weisman, R. B. *Nano Lett.* **2005**, *5*, 975-979.

(36) Wang, F.; Dukovic, G.; Brus, L. E.; Heinz, T. F. *Phys.Rev.Lett.* **2004**, *92*, 177401.

(37) Weisman, R. B.; Bachilo, S. M. *Nano Lett.* **2003**, *3*, 1235-1238.

(38) Dukovic, G.; Wang, F.; Song, D. H.; Sfeir, M. Y.; Heinz, T. F.; Brus, L. E. *Nano Lett.* **2005**, *5*, 2314-2318.

(39) Pedersen, T. G. *Carbon* **2004**, *42*, 1007-1010.

(40) Finnie, P.; Homma, Y.; Lefebvre, J. *Phys.Rev.Lett.* **2005**, *94*.